Characteristics and timing of hydrothermal fluid circulation in the fossil Pyrenean hyperextended rift system: new constraints from the Chaînons Béarnais (W Pyrenees)

Characteristics and timing of hydrothermal fluid circulation in the fossil Pyrenean hyperextended rift system: New constraints from the Chaînons Béarnais (W Pyrenees).

[1-2]Incerpi N., [2]Manatschal G., [1]Martire L., [3]Bernasconi S.M., [4]Gerdes, A., [1]Bertok C.

[1]Dipartimento di Scienze della Terra, Università degli Studi di Torino, Via Valperga Caluso 35, 10125 Torino, Italy. **nincerpi@unito.it** - mobile phone: +39 340 1024842 - ORCID: https://orcid.org/0000-0002-3446-4829

[2]CNRS-UMR 7516, Institut de Physique du Globe, Université de Strasbourg, 1 rue Blessig, 67000 Strasbourg, France

[3]Department of Earth Sciences, ETH Zürich, Sonneggstrasse 5, 8092 Zürich, Switzerland

[4]Institut für Geowissenschaften, Facheinheit Mineralogie - Petrologie und Geochemie, Altenhöferallee 1D-60438 Frankfurt am Main, Germany

Keywords: Hydrothermal fluids; Hyperextended rift system; Pyrenees; Diagenetic evolution; Mauléon Basin

Aknowledgement: The research was financed through a grant to Gianreto Manatschal by ExxonMobil, Petrobras S.A. and MM4 Consortium (BP, Conoco Phillips, Statoil, Petrobras, Total, Shell, BHP-Billiton and BG). Universita Italo-Francese/Universite Franco-Italienne is also thanked for the Bando Vinci 2014 grant (C2-190) to Nicolo Incerpi.

Corresponding author: Nicolò Incerpi nincerpi@unito.it

ABSTRACT

The evolution of hyperextended rift systems is linked to complex tectonic processes in which fluid activity is much more important than previously thought. This study sheds light on the fluid-sediment interactions within the distalmost parts of the Mauléon-Arzacq hyperextended basin (Western Pyrenees) focusing on the post-depositional modifications of pre- to syn-hyperextension sediments due to hydrothermal fluids. Strong field- and petrography-based evidence demonstrates the presence of fluid-related products affecting the Jurassic to Cretaceous sediments exposed in the Chaînons Béarnais (easternmost Mauléon basin). These are supported by new U-Pb dating of carbonates and microthermometry of fluid inclusions showing temperatures of up to 250°C and highly depleted $\delta^{18}O$ and strongly enriched $^{87}Sr/^{86}Sr$. Two main stages of fluid activity can be defined: i) a carbonate-rich stage leading to fabric-destructive replacement dolomitization of the pre-rift carbonates, widespread hydro-fracturation giving rise to different types of hydraulic breccias cemented by multi-phase dolomite and calcite dated at ~ 96 Ma; and ii) a Na-SiO_2-rich stage associated with authigenic albite and quartz, mainly affecting syn-rift deposits. Finally, the occurrence of dolomitic marbles and mylonites provide evidence for strong recrystallization and ductile shearing affecting the sediments during the latest stages of hyperextension at ~ 94 Ma. The Chaînons Béarnais represent a primary target to investigate fluid-rock interactions linked to extensional tectonics that can be used as an analogue to compare to other fossil rift systems (e.g. Adriatic paleo-rifted margin) or present-day magma-poor, hyperextended rifted margins (e.g. Iberia-Newfoundland).

1. INTRODUCTION

The Pyrenean-Bay of Biscay rift system has been extensively investigated using onshore and offshore seismic surveys, well data and field work. Many of these studies tried to decipher the kinematic evolution of the Iberian-European plate boundary and the related evolution of the rift basins and their later reactivation during the Pyrenean orogenesis (Asti et al. 2019; Saspiturry et al. 2019; Garcia-Senza et al. 2019). Despite of this, some key aspects concerning the extensional evolution are still not fully constrained. One of this is the link between the syn-rift fluids, the diagenetic evolution of the pre- to syn-hyperextension sediments and the evolving thermal state during hyperextension. Fluid circulation at hyperextended rift systems is a relatively "new" subject that has been rigorously taken into account only in the last few years (Alps: Pinto et al. 2015; Incerpi et al. 2017, 2018, 2019; Coltat et al. 2019; Gulf of Suez: Hollis et al. 2017; Pyrenees: Salardon et al. 2017; DeFelipe et al. 2017; Corre et al. 2018; Quesnel et al. 2019).

The evolution and formation of passive rifted margins is strictly linked to different geological processes (e.g. magmatic, tectonic and sedimentary) in which fluids play an essential role. Nonetheless, their physico-chemical properties, their pathways and source areas are still less studied and understood expecially in the sedimentary environment. Due to the oceanographic surveys (e.g. IODP/ODP) and the discoveries of hydrothermal vents at present-day ocean ridges, as well as the occurrence of widespread serpentinization processes, the relevance and spatial abundance of fluid activity in response to the late stage of continental rifting and oceanization are relatively well understood (Kelley et al., 2001; Boschi et al., 2006; McCaig et al., 2007; Kelley and Shank, 2010; Edmonds, 2010; Pinto et al. 2015, 2016; Hensen et al., 2019). On the contrary, little attention has been paid to the study of such activity in the more internal part of the continental margins (proximal and distal domains) where the pre-mantle exhumation history is preserved. Only few ODP (Ocean Drilling Program) drill holes are available, which, even if far to be considered exhaustive, shed light on the importance of fluid circulation and related mineralization (e.g. dolomitization at ODP Leg 103; Boillot et al., 1988). It is commonly accepted that fluids have a strong influence on the mass and heat transfer within the rock column, development/reduction of permeability as well as maturation of organic matter (e.g. Renard et al. 2019). Therefore, the understanding of fluid activity, especially its timing and composition, is crucial not only for academia but also for industry. Present-day rifted margins obviously represent the main target for this kind of studies. The difficulty to obtain direct observations at deep-water margins (e.g. most data sets are proprietary) makes that remnants of hyperextended systems preserved in collisional orogens have been used as analogues (e.g. Beltrando et al. 2014; Tugend et al. 2015; Epin et al. 2018; Saspiturry et al. 2019; Ribes et al. 2019a). This study focuses on the eastern Mauléon-Arzacq basin exposed in the western French Pyrenees and more precisely in the so-called Chaînons Béarnais (Fig. 1), where well-preserved features of the former Pyrenean hyperextended rift system are exposed (Jammes et al. 2009). Here, the relationship between crustal and mantle derived rocks, the Mesozoic sediments and the hyperextended-related structures crop out and, importantly, are not overprinted by metamorphic reactions during the Pyrenean reactivation (Lagabrielle et al. 2010; Clerc et al. 2015; Tugend et al. 2015). The aim of this study is to provide evidence of rift-related high-T fluid activity as well as ductile deformation leading to post-depositional modifications (veining, hydraulic brecciation, dolomitization, silicification) taking place within the pre- and syn-hyperextension sediments preserved in the eastern termination of the Mauléon Basin. Based on an original multidisciplinary dataset (fieldwork, petrography, stable isotopes geochemistry, fluid inclusions micro-thermometry and U-Pb dating on carbonates) and on the comparison with well-constrained examples from present-day margins and fossil analogues

(e.g. Incerpi et al. 2019; Picazo et al. 2019; Corre et al. 2018; Salardon et al. 2017; Bayrakci et al. 2016; Boillot et al. 1988), different lines of evidence will point to the occurrence of a strong hydrothermal activity during rifting.

2. GEOLOGICAL SETTING

2.1 The Bay of Biscay-Pyrenean rift system

The present-day Pyrenean-Bay of Biscay rift system resulted from multiphase Triassic to Cretaceous rifting events, which led to the formation of hyperextended basins and oceanic crust during the Late Aptian to Cenomanian in the western Bay of Biscay (Fig. 1; Jammes et al. 2009; Filleaudeau et al. 2012; Clerc and Lagabrielle 2014; Mouthereau et al. 2014; Tugend et al. 2015; Vacherat et al. 2016). This rift system was reactivated during latest

Cretaceous (Campanian to Santonian; ~84Ma) in response to the convergence of the European and Iberian plates. Lithospheric break-up and seafloor spreading in the Bay of Biscay occurred simultaneously to hyperextension further to the east in the Pyrenean domain. These processes are widely described both offshore (Parentis basin: e.g. Roca et al. 2011) and onshore (e.g. the Aulus basin: e.g. Clerc et al. 2012; the Arzacq-Mauléon basin: e.g. Masini et al. 2014; and the Basque-Cantabrian basin; e.g. Pedreira et al. 2007). Due to the inversion of the Mesozoic basins during the Pyrenean orogenesis, the basal parts of the former hyperextended rift basins were uplifted and emplaced over the former proximal parts of these basins. This is best documented in the Mauléon-Arzacq Basin that represents a reactivated and partly exposed analogue of the offshore Parentis Basin (Jammes et al. 2009, 2010a, b). Several authors suggested the occurrence of rift-related detachment faults in the western Mauléon Basin (e.g., Ducasse and Vélasque 1986; Johnson and Hall 1989a, b; Claude 1990; Jammes et al. 2009; Lagabrielle et al. 2010; Masini et al. 2014) that juxtaposed exhumed mantle, mid and upper crustal rocks against pre-, syn and post-rift sediments.

Because of the occurrence of several rift phases along the Mesozoic evolution of the Pyrenean rift system, it is important to clarify that only the last rift stage evolved into the mid-Cretaceous hyperextension (HE), which led also to mantle exhumation. In this frame, this work focuses on the pre- and syn-HE sediments (*sensu* Masini et al. 2014).

2.2 The HT-LP metamorphism: features and distribution

One of the most interesting features characterizing the Late Aptian to Cenomanian hyperextension phase is the occurrence of a HT-LP metamorphic event (Fig. 2; e.g. Clerc and Lagabrielle 2014) affecting the pre- to syn-HE

sediments distributed along the North Pyrenean Zone (NPZ). This thermal event is spatially and temporally linked to extreme crustal thinning ultimately leading to mantle exhumation as testified, among other lines of evidence, by several outcrops of granulites and sub-continental peridotites along the NPZ (e.g. Lagabrielle and Bodinier 2008).

Clerc and Lagabrielle (2014) defined 3 different domains based on the T_{max} recorded by pre- and syn-HE Mesozoic sediments in the NPZ (Fig. 2b): i) the Western domain showing low-grade metamorphism with temperatures generally lower than 350°C. The highest values occur close to mantle rocks and Paleozoic basement; ii) the Central domain showing temperatures of 300°C to 450°C, only locally exceeding 550°C close to mantle rocks and decreasing toward the west; and iii) the Eastern domain showing the highest metamorphic grade with temperatures up to 600°C.

Several geochronological studies dated this metamorphic event within the Albian-Santonian range (105-85 Ma; Fig. 3 in Clerc et al. 2015 and references therein). Moreover, a hydrothermal alteration leading to albitization and de-quartzification of the North Pyrenean basement rocks and the formation of massive talc deposits during the late Aptian to early Cenomanian (Schärer et al. 1999; Boulvais et al. 2007; Poujol et al. 2010; Quesnel et al. 2019) at temperatures ranging from 250°C (Boulvais et al. 2006) to more than 500°C occurred (sodic-calcic metasomatism; Fallourd et al. 2014).

All along the inner NPZ, Triassic to Albian-Cenomanian rocks bear evidence of intense ductile deformation generally transposing the original stratification of the Mesozoic meta-sediments. Stretching lineations made up of HT-LP minerals (scapolite) occur within mylonitized marbles. Lastly, the Northern Pyrenean realm shows evidence for polyphase magmatic activity including: i) tholeiitic dolerites of Triassic age, generally referred to as "ophites" (Montigny et al. 1982; Azambre et al. 1987), and ii) small intrusive and effusive Cretaceous alkaline magmatic rocks (Montigny et al. 1986; Azambre et al. 1992; Rossy et al. 1992). The age of the Cretaceous magmatism is often constrained by stratigraphic correlations with the sedimentary formations in which volcanic or intrusive rocks are observed (San Miguel de la Camara 1952; Rossy 1988; Castanares et al. 1997; Lopez-Horgue et al. 1999; Castanares et al. 2001; Lopez-Horgue et al. 2009). Radiometric ages are also available ranging from 113 to 85 Ma (Golberg et al. 1986; Montigny et al. 1986; Henry et al. 1998).

2.3 The Chaînons Béarnais: the distalmost Pyrenean rift domain

The Chaînons Béarnais consist of three E-W trending "ridges" made up of Upper Triassic- to Lower Cretaceous sediments and local occurrences of mantle and crustal rocks that are folded and thrust. They are preserved at the easternmost termination of the Mauléon Basin (Figs. 1b-3a) and, from north to south, are referred as: Mail Arrouy, Sarrance and Layens. The base of the Mesozoic sequence is in most cases represented by the Triassic Keuper facies with shales, evaporites, breccias and ophites, overlain by Jurassic to Aptian platform limestones and dolomites. These sediments represent the pre-HE sequence (*sensu* Masini et al. 2014), now entirely detached from its Palaeozoic basement (Lagabrielle et al. 2010; Teixell et al. 2016), which is only locally preserved at the base of the Mesozoic succession. Several authors (Jammes et al. 2009; Lagabrielle et al. 2010; Masini et al. 2014; Teixell et al. 2016) interpreted the Chaînons Béarnais as extensional allochthons lying over both hyperextended continental crust and exhumed mantle (Fig. 1). Lagabrielle and Bodinier (2008) and Jammes et al. (2009, 2010) proposed that these mantle rocks were exhumed, reworked and redeposited during Albo-Cenomanian time (e.g. during hyperextension).

The study area, located few kilometers west of the town of Lourdes, is characterized by a folded pre-HE Keuper to Kimmeridgian stratigraphic sequence. Within the area (Fig. 3b), it is not possible anymore to distinctly recognize the three ridges since Mail Arrouy and Sarrance are merged.

2.4 New lithostratigraphic names

Fluid-related products have been found at different stratigraphic levels within the study area (Fig. 3b) in both the pre- and syn-HE sediments. As shown in Fig. 3b, new names and ages for some lithostratigraphic units will be adopted compared to those proposed in the *Lourdes map sheet* by Casteras et al. (1970) which were strictly based on chronostratigraphy. The pre-HE Kimmeridgian and Callovian-Oxfordian sediments will be here named Black Dolomites (BD) and Black Limestones (BL), respectively. The former Ophites and Rhaetian-Lower Hettangian sediments are here considered as syn-HE sediments named Sedimentary Breccias (SB) representing reworked material redeposited during the HE event (see text for details and interpretation).

3. METHODS AND MATERIALS

Field observations and sampling were performed at the easternmost termination of the Chaînons Béarnais (Fig. 3a). Petrographic studies (optical microscopy and cathodoluminescence; CL) on polished thin sections and *in situ* quantitative microprobe analyses (EDS) were performed at the University of Turin (Italy). Carbon and oxygen isotopic compositions of the carbonates were measured at the ETH Zürich (Switzerland; Breitenbach and

Bernasconi, 2011). Fluid inclusions (FIs) petrography and micro-thermometry of primary FIs have been performed on bi-polished thin sections (100 µm) at the University of Turin (Italy). Sr isotope compositions and U-Pb dating on carbonates (Gerdes and Zeh, 2006; 2009) have been carried out at the University of Frankfurt (Germany). Further details on each method are given as Online Supplementary Material.

4. EVIDENCE OF FLUID ACTIVITY

4.1 BDU - Black Dolomite Unit (Callovian-Oxfordian)

This lithostratigraphic unit is composed of coarsely to very coarsely crystalline, pyrite-rich, black dolostones that do not show a well-defined bedding and can reach, in the *Lourdes map sheet* (Castéras et al. 1970), a maximum thickness of 400m.

In the study area, the BDU is characterized by subhedral to euhedral, non-luminescent under CL, replacement dolomite whose crystals can reach 300µm in size. These dolostones show different degrees of internal disruption. Where less deformed, the BDU is affected by randomly oriented, few µm wide, fracture sets (only visible by CL) filled by dolomite cement, bright orange under CL (Figs. 4a-b). These micro-fractures usually occur along crystal contacts even if they also cut through them. Locally, some originally open spaces occur. They are cemented by dolomite whose crystals, 100-200 µm large, show a bright orange, very poorly zoned CL luminescence. By their features, these portions of the rock mass can be considered as incipient crackle breccias (*sensu* Morrow 1982).

Where the deformation is stronger, polygenic mosaic to rubble breccias (*sensu* Morrow 1982) occur (Figs. 4c-d). They are made up of millimeter- to some centimeter-large clasts of finely to coarsely crystalline dolomite, angular in shape and dull in CL. Within some clasts, ooids are still recognizable. The clasts themselves show different degrees of internal deformation: from almost preserved dolostones to strongly fractured and brecciated clasts cemented by bright orange luminescing dolomite. The mosaic to rubble breccias are cemented by two generations of saddle dolomite. The first, almost isopachous and up to 500 µm thick, shows CL zoning from bright to dark orange. Commonly, in between the clasts and the first dolomite cement, a geopetal filling with dolomitized fine-grained sediment occurs (Figs. 4e-f). The second cement, finally, is still dolomite and is characterized by a bright, poorly zoned, orange luminescence. In few cases, a third cement made up of dark orange/brown luminescing calcite occurs. It occurs as calcite spar with crystal sizes ranging between tens to hundreds of microns.

The whole breccias (e.g. clasts and cements) are then crosscut by several randomly oriented dolomite veins that are recognizable only by CL observation. They occur as tens to hundreds of microns wide fractures filled with an

almost homogeneous orange dolomite cement. Lastly, tens of microns wide calcite veins, with a dark brown to dull luminescence in CL, are present.

4.2 BLU - Black Limestone Unit (Kimmeridgian)

The BLU crops out in the central part of the study area and shows an overall thickness of 200-300 meters (Casteras et al. 1970). It is made up of fine-grained, well-bedded limestones alternated with black to reddish marly limestones. Locally, it is dolomitized. These limestones are microsparitic, dark orange in CL and cut by dolomite and calcite veins, hundreds of µm wide. Bivalve shells, echinoderm and gastropod fragments, oncoids and cortoids are preserved even if recrystallized. Some bioclasts are coated by pyrite. Casteras et al. (1970) described part of the BLU in the study area as "metamorphosed limestones" made up of white, scapolite-rich marbles (red dashed area in Fig. 3b). However, we explain below that the white marbles represent only one of the several post-depositional modifications experienced by the BLU. Locally, the BLU is characterized by the occurrence of several, up to 300 µm long, unusual structures made up of fibrous calcite growing perpendicularly to and encasing fibrous aggregates of Mg-rich alumino-silicates (Figs. 5a-b). Raman spectroscopy investigations revealed that such silicates are hydrated and characterized by spectra similar to that of talc and chlorite.

4.2.2 The breccias

Three types of clast-supported hydraulic breccias differing for their clasts and cement composition were observed (Fig. 6).

1) The type 1 breccia is made up of centimeter- to some decimeter-sized angular clasts constituted of microsparitic limestones cemented by very coarse, sparry calcite crystals that can reach some centimeters in size (Figs. 6a-b). Locally, a dolomite rim, zoned in CL, fringes the clasts and is always coupled with a hundred of µm thick rim of dolomitized fine-grained sediment. Both the clasts and the calcite cement show a homogeneous orange CL luminescence.

2) The type 2 breccia is made up of clasts of coarsely crystalline dolostones of the BDU (Figs. 6c-d). The clasts, angular in shape and up to 5 cm in size, are cemented by a fine-grained (few tens of microns), homogeneous orange/brownish luminescing calcite. Within the clasts, some cavities are cemented by type 1 dolomite already described in the BDU. Some detrital dolomite crystals (200 µm in size), still encased within the calcite cements, show a few µm large, bright orange, dolomite overgrowth, evidenced only by CL investigations. Within the calcite cement, some large detrital crystals (2,5 mm large) made up of a former dolomite cement are also present.

Locally, type 2 breccia clasts are characterized by a stronger internal deformation giving rise to poorly sorted, brecciated textures composed of hundreds of µm large, almost rounded clasts within a bright orange luminescing dolomite cement. These portions of the rock are also crossed by different, diachronous, vein sets cemented by dolomite and calcite. The former is characterized by a poorly zoned orange luminescence, whereas the latter shows well defined, yellow to brownish, concentric zoning.

3) The third type is a polymict breccia made up of larger clasts, cm to dm in diameter, bluish on the weathered surface composed of micro-crystalline limestones, and smaller clasts, mm to cm in size, made up of fine grained dolostones. The spaces among clasts are filled with a complex cement composed of: i) coarse grained dolomite crystals (up to 500 µm) with dark orange, poorly zoned, luminescence, and ii) yellowish to dark orange luminescing sparry calcite (300 µm) (Figs. 6e-f).

4.2.3 Mylonites and marbles

Strongly recrystallized carbonate rocks occur along the talweg of the Genie Longue creek (Fig. 3b). In the few spots where they were observed, they look discordant with the surrounding lithotypes (BLU and their modifications). The stratigraphic or tectonic contact with these sediments has never been observed due to poor exposure.

These rocks show a regular and planar foliation evidenced by alternating dm- to m-large whitish and bluish layers (Figs. 7a-b). Whitish layers are composed of finely crystalline dolomite with some scattered authigenic quartz crystals (up to 400 µm large; Fig. 7d) that poikilotopi~~k~~cally include the carbonate matrix. Sulphide and opaque minerals also occur (from few µm to tens of µm). Fine grained quartz is also present between the dolomite crystals. Under cathodoluminescence and excluding the non-luminescent quartz, the rock appears with a homogeneous orange color. The bluish layers, still made up of fine-grained dolomite, contain stretched and parallel to the bedding polycrystalline dolomite porphyroclasts. Quartz is still present both in the porphyroclasts and in the matrix. Relicts of former scapolite (Fig. 7c), 500 µm large and presently completely replaced by fine grained aggregates of K-rich alumo-silicates occur. Such porphyroblasts include poikilotopically the carbonate matrix. Despite the mylonitic appearance, the microstructures reveal a static recrystallization postdating the deformation.

Out of the riverbed and in an area comprised between the Genie Longue and Braque creeks before their confluence, few spotty occurrences of white, coarsely crystalline dolomite marbles were found (Figs. 7e-f). The crystals, up to 500 µm, are characterized by a dark orange CL luminescence. Brighter luminescing zones correspond to crystal

contacts. On the whole, the rock is made up of almost equant crystals with sutured boundaries; only locally, planar boundaries occur. This microstructure is similar to that observed within the porphyroclasts of the mylonites. Where observed, the marbles are massive and do not show a well-defined bedding nor a foliation.

4.3 SBU - Sedimentary Breccia Unit (post-Kimmeridgian)

Along the southern ridge of the study area as well as its northeastern part, evaporites, ophites and sedimentary breccias are exposed. The ophites and the evaporites were assigned to the Keuper, whereas the breccias were described as Rhaetian to Sinemurian in age (Casteras et al. 1970). New observations allowed three types of sedimentary breccias to be distinguished: ophitic monomictic, polymictic and carbonate monomictic. The Ophite unit, conversely to what has been proposed in the *Lourdes map sheet* (Casteras et al. 1970), occurs as monomict clast-supported sedimentary breccia, with an overall thickness of about 20 meters. It is constituted exclusively of almost rounded ophitic clasts ranging in size from some centimeters to around a meter. Laterally, the ophitic breccia passes to polymict sedimentary breccias mainly composed of carbonate clasts, and subordinately ophitic clasts (Figs. 8a-c). The clasts are mm- to cm-large, even if some larger, mainly ophitic clasts can reach a few decimeters. Compositionally, the carbonate clasts are made up of micritic to microsparitic limestones, oolitic limestones showing different degrees of dolomitization, and finely to coarsely crystalline dolostones. Locally gastropods and bivalve shells are still recognizable, even if recrystallized. Dolomite veins, confined within the clasts, are common and characterized by orange luminescencing crystals, up to few hundreds of µm in size. Among the siliciclastic material, clasts made up of polycrystalline quartz occur (crystals size up to 10 µm). The matrix of this mixed breccia is a sandstone made up of the same material of the clasts and detrital quartz. It is important to note the occurrence of authigenic quartz (30-40 µm large) and albite that poikilotopically grow over the matrix, including tens of µm-sized carbonate crystals (Figs. 8d-f). Albite, chemically almost pure, is euhedral and randomly oriented, up to 2 mm long, showing the characteristic Roc Tourné twinning and absence of luminescence under CL. Furthermore, authigenic opaque minerals (sulphides up to 500 µm large) are widespread. Lastly, dolomite veins crosscut the entire breccia body (e.g. both clasts and matrix).

A third sedimentary breccia type occurs, stratigraphically above the previously described ophitic and polimict breccias. It is clast-supported and composed solely of carbonate clasts within a matrix that shows the same features of the polimict breccias (e.g. authigenic quartz, albite and opaque minerals; Figs. 8e, f). The clasts, ranging in size from few mm to cm, are made up of micrites, microsparitic limestones and fine grained laminated dolostones preserving the pristine features of the rock (e.g. shrinkage pores, fossils). Some clasts show borings possibly

referable to *Lithophaga* at the edge. Within some clasts, dolomite veins occur. Other clasts, conversely, are strongly recrystallized and the recognition of pristine features is no longer possible. It is the case of coarse grained, sucrosic dolostones that under CL are almost non-luminescent and preserve some cavities filled with orange luminescing dolomite cement. By their petrographic and CL features, they are clearly referable to the BDU. Few dolomite veins, characterized by a concentric CL zoning alternating dull and bright orange CL zones, cut through the whole rock mass.

Because of the occurrence of clasts derived from the BDU in the SBU as well as the occurrence of authigenic albite and quartz (see further details in Discussion), the SBU has to be younger than both BDU and BLU (Fig. 9).

5. ANALYTICAL DATASET

5.1 Fluid inclusion microthermometry

Homogenization temperatures (T_h) of primary fluid inclusions were measured on calcite and dolomite cements of: i) hydrofracturing breccias of BDU (highest frequency 230-240°C); ii) hydraulic breccias of types 1-3 of BLU (highest frequency 240-250°C and 180-190°C, respectively); and iii) marbles and mylonites (highest frequency 240-250°C). The results are shown in Fig. 10a and Table 1. Because of the very small size of primary fluid inclusions it has not been possible to perform cooling cycles in order to get the salinity of inclusions.

5.2 Oxygen and Carbon isotopes

Oxygen and carbon isotope analyses are reported in Fig. 10b and Table 1. The host BDU dolomite shows positive $\delta^{13}C$ (2.27 ‰ to 3.29 ‰ VPDB) and negative $\delta^{18}O$ values (-3.37 ‰ to -7.79 ‰ VPDB). The BDU dolomite cement has slightly positive $\delta^{13}C$ values (1.38 ‰ to 2.16 ‰ VPDB) and markedly negative $\delta^{18}O$ (-8.60 ‰ to -12.10 ‰ VPDB).

The BLU host limestones show slightly positive $\delta^{13}C$ values between +0.5 ‰ to +3 ‰ and negative $\delta^{18}O$ ranging from 0 ‰ to -8 ‰. The BLU calcite cement of breccia type 1 has $\delta^{13}C$ values in the range -2 ‰ to +2 ‰ and markedly negative $\delta^{18}O$ (-6 ‰ to -14 ‰).

The marbles show positive $\delta^{13}C$ values (about +3 ‰) and negative $\delta^{18}O$ (-7 ‰). The whitish layers of the mylonites have slightly positive $\delta^{13}C$ values (1.67‰) and slightly negative $\delta^{18}O$ values (-1.11 ‰). The bluish layers show always slightly positive $\delta^{13}C$ values while $\delta^{18}O$ values are more depleted (about -7 ‰).

Calculations of the isotopic composition of fluids responsible for dolomite and calcite precipitation, by using the temperatures of carbonate precipitation determined with fluid inclusion microthermometry and using the equations of Horita (2014) for dolomite and Anderson and Arthur (1983) for calcite, provide markedly positive oxygen isotope values for the calculated fluids of up to +9 ‰ vs. SMOW for dolomite and up to +12 ‰ (VSMOW) for calcite. The $\delta^{13}C$ values of all the analyzed samples show values in the range of normal marine sedimentary carbonates. The $\delta^{18}O$ of the carbonates range from 0 to -14 ‰ (PDB). Based only on the $\delta^{18}O$ values, two main groups of data can be distinguished: the host limestones and the replacement dolostones (dots in Fig. 10b) which show relatively higher values, and calcite and dolomite cements in hydraulic breccias (rhombs in Fig. 10b) with more ^{18}O-depleted values. Comparing our dataset with those of Incerpi et al. (2019) for the Adriatic paleo-rifted margin and Boillot et al. (1988) for the present-day Galicia margin, the overall trend is similar (Fig. 10c): the replacement minerals are always less ^{18}O-depleted than the void-filling cements in veins and breccias.

5.3 Sr isotopes

The $^{87}Sr/^{86}Sr$ ratios (Table 1) in BDU and BLU hydraulic breccias (clasts, dolomite and calcite cement), mylonites and marbles show values from 0.70972±0.00024 to 0.73204±0.00051, significantly higher than Jurassic-Cretaceous seawater (highest value 0.70780; McArthur et al., 2012).

5.4 U-Pb datings

U-Pb datings have been performed on hydraulic breccia BDU clast (143.5 ± 9.1 Ma) and BLU clast (122 ± 16 Ma); hydraulic breccias dolomite cement (95.7 ± 3.4 Ma; 102 ± 40 Ma); mylonite (93.9 ± 3.5 Ma; 90.3 ± 4.9 Ma). The results are shown in Figs. 11-12 and Table 1.

6. DISCUSSION

6.1 Constraints on the fluids' characteristic

6.1.1 The hydrothermal dolomitization

The coarse-grained replacement dolomite of the BDU dolostones, even if not constrained by fluid inclusion micro-thermometry, could be related to hot fluid circulation as indicated by the low $\delta^{18}O$ values. Indeed, $\delta^{18}O$ values for replacement dolomite are lower than those documented in modern settings, where dolomite is forming (0 to +4‰; Tucker and Wright 1990; Meister et al. 2013). Moreover, Incerpi et al. (2019) documented coarse-grained replacement dolomites, within Triassic dolostones of the Adriatic rifted margin preserved in the Central Alps that

are due to high-T fluids strictly related to the rift evolution. The T_h measured in this study for the different analysed mineral phases show values (from 180 to 250°C for void-filling cements) which cannot be explained by the only sedimentary overburden at the time of their formation, as the maximum estimated thickness of sediments at that time would be ~ 4 km. Hydrothermal fluid circulation is then clearly documented associated to anomalous thermal gradient at this stage of rifting (REFERENCES). Moreover, the occurrence of internal sediment among clasts of the hydraulic breccias requires a fracture network connected with the seafloor to allow the infiltration of sediment and implies that the fluid circulation products (e.g. hydraulic brecciation, veining and replacement) were superficial.

Different processes may be invoked for the positive oxygen isotopic signature calculated for fluids in equilibrium with the cements of the hydraulic breccias: evaporative enrichment of the infiltrating waters (e.g. McKenzie 1991), clay mineral diagenesis (e.g. Hensen et al. 2007) and water-rock interaction with silicate minerals of siliciclastic and crystalline rocks (e.g. Haeri-Ardakani et al. 2013). Considering the model of Jammes et al. (2009), where the Chaînons Béarnais are considered to be extensional allochthons in a deep-water setting, the only reasonable source of fluid feeding the hydrothermal system is seawater. However, the occurrence of thick Keuper evaporites at the base of the Mesozoic sedimentary column likely provided the main contribution in determining such isotopic enrichment. Furthermore, an interaction with basement rocks must be considered as demonstrated by the highly enriched Sr isotopes. Recently, Corre et al. (2018) and Salardon et al. (2017) described, in the pre-HE sedimentary sequences of the western Chaînons Béarnais, similar fluid-driven diagenetic processes invoking the occurrence of HT fluids during the hyperextension phase of rifting. Boillot et al. (1988) reported similar diagenetic evolution within the extensional allochthons drilled in the distal domain of the Galicia margin (ODP Leg 103).

Even if seawater is *per se* a dolomitizing fluid (e.g. Land, 1985; Purser et al., 1994; Machel, 2004), an additional source of Mg can be invoked. Based on chemical exchanges during serpentinization (Pinto et al. 2015) and the occurrence of serpentinized lherzolites in the Chaînons Béarnais (Lagabrielle et al. 2010), the source of Mg favoring, at least partly, the diffuse dolomitization could also be related to mid-Cretaceous serpentinization processes (Masini et al. 2014). The tectonic activity leading to hyperextension and mantle exhumation was also the trigger responsible for the erosion of the allochthons and the subsequent deposition of the Sedimentary Breccias Unit (e.g. hangingwall-derived breccias as the “Alpine” Bardella Fm. in Masini et al., 2011; Ribes et al. 2019a, b). This stage, notably, is linked to a marked change in the chemistry of the fluid system, which led to the precipitation of authigenic albite and quartz within the SBU (Fig. 9). Such “jump” from a carbonate- to silica-

dominated fluid system has been already described and well-constrained in the Adriatic (Swiss Alps; Incerpi et al. 2017, 2019) and European paleo rifted margins (Ligurian Alps, unpublished data).

6.1.2 Albitization of the Sedimentary Breccia Unit (SBU)

The occurrence of authigenic albite within the SBU is noteworthy. Despite albitization is a well-known process in green schist metamorphic rocks, it is also quite common in high-grade diagenetic carbonate rocks (Spötl et al. 1999). The resulting albite shows euhedral habit, pure chemical composition, the peculiar Roc-Tourné twinning (Kastner 1971) and absence of CL luminescence due to its chemical purity (Richter et al. 2002). Furthermore, the grains poikilotopikally included within the authigenic albites represent remnants of the host rock and provide one more distinctive feature with respect to the magmatic ones (Kastner 1971). All of these requisites characterize the albite crystals studied in this work (Fig. 8) providing evidence for a post-depositional growth. Rais et al. (2008) proposed high-T (~200-300°C) for Na- and Si-rich albitizing fluids, which are compatible with those measured in this study on other hydrothermal mineral phases. On a regional scale, albitization has been described in the eastern Pyrenees as a product of fluid/rock interactions occurring during syn-HE Na-Ca metasomatic event dated at about 100 Ma (Boulvais et al. 2007; Poujol et al. 2010; Fallourd et al. 2014).

Finding of BDU and BLU-derived material reworked within the SBU has strong implications on its age as the breccias cannot be older than the youngest rocks that compose the clasts, i.e. Callovian-Oxfordian. Therefore, the SBU is likely to be considered as syn-HE unit related to the reworking of pre-HE rocks during the mid-Cretaceous hyperextension. Such hypothesis is also supported by the post-depositional albitization affecting the breccias, which, as just said, have been dated as mid-Cretaceous.

6.2 Constraints on the timing of fluid activity

6.2.1 The U-Pb dating on carbonates

U-Pb dating of the dolomitized host BDU and BLU carbonates shows Berriasian (143.5 ± 9.1 Ma) to Aptian (122 ± 16 Ma) ages (Figs. 11-12). The former may be interpreted as a dolomitizing event taking place during the stretching phase of the Pyrenean rift system. The latter, conversely, matches with the onset of hyperextension rifting phases. The most precise U-Pb dating refers to the cements of hydraulic breccias and the mylonites. As shown in Figs. 11-12 and Table 1, the values show very low 2σ. These Cenomanian-Turonian ages represent the very last moment when hyperextension and mantle exhumation took place in the Mauléon Basin.

Considering the paleogeographic position of the Chaînons Béarnais (Jammes et al. 2009; Teixell et al. 2016), the U-Pb data confirm and strongly support the occurrence of conspicuous fluid circulation within the allochthons, when the deformation was actively working at the upper/lower plate boundary. Replacement dolomitization and subsequent hydraulic brecciation taking place before and during hyperextension has been strongly constrained in both the Adriatic paleo-rifted margin (Incerpi et al. 2017; 2018; 2019) and the Pyrenean rift system (Mauleon Basin: Salardon et al. 2017; Corre et al. 2018; Aquitaine Basin: Renard et al. 2019). The following evolutionary model for the study area can then be proposed:

1) Carbonate-rich stage:

- First event of circulation of dolomite-saturated fluids leading to pervasive and fabric-destructive dolomitization of the BDU.

- Second event of circulation of dolomite-saturated fluids and formation of crackle, mosaic and rubble breccias within the BDU. These fluids, strongly overpressured, could also be responsible for the formation of hydrofracturing breccias type 3 within the overlying BLU. Since clasts are made up of both BDU and BLU, hydrofracturing had to occur at least in post-Kimmeridgian time. U-Pb dating, further constrains the age of the brecciation event to be Albian to Cenomanian in time.

- First phase of circulation of calcite-saturated fluids as documented by the cement of the mosaic to rubble breccias of the BDU and that of breccia types 1, 2 and 3 within the BLU.

2) Na- and SiO_2-rich stage:

- First event of circulation of Na- and Si-rich fluids shown by poikilotopic growth of quartz and albite over the matrix and clasts of the SBU.

6.3 The upper/lower plate boundary

The Chaînons Béarnais ridges, interpreted as extensional allochthons, represent the most distal portions of the Pyrenean rift system (Figs. 3, 13). As demonstrated by recent studies (Brune et al. 2014; Hart et al. 2017), this portion of the rift systems that includes the upper/lower plate boundary is the place where the highest heat flow is localized due to the uprising mantle along exhuming detachment faults (e.g. Lescoutre et al. 2019). Such peculiar

configuration leads to very high geothermal gradients (up to 100°C/km; Hart et al. 2017; Sun et al. 2018a, b) exactly where allochthons are forming. Lescoutre et al. (2019) demonstrated, on the base of the heat flow and vitrinite reflectance measurements in the Mauléon Basin, that the thermal state of distal rift domains could be used as fingerprint to define the polarity of the rift system itself (e.g. defining the lower and upper plates). By their observations, they recognized the occurrence of a thermal asymmetry mirroring the structural asymmetric architecture typical of magma-poor rifted margins.

Lagabrielle et al. (2016) interpreted the occurrence of marble mylonites, cataclastic and sedimentary breccias in the Lherz area in the Eastern Pyrenees as a response of both ductile and brittle deformation of the pre-rift sediments related to such thermal perturbation during exhumation. Our observations from the Western Pyrenees seem to support this interpretation. Ductile deformation, here described for the first time in the Mauléon Basin, affected an already metamorphosed sedimentary sequence as shown by the occurrence of marbles porphyroclasts within the mylonites. Furthermore, petrographic observations revealed the annealing of the mylonitic fabric pointing to the occurrence of thermal overprint which outlasted the deformation. This interpretation is supported by the results obtained by Vacherat et al. (2014). Almost coevally (see U-Pb ages), but at shallower levels, brittle deformation associated with strong fluid circulation lead to hydraulic brecciation and veining. Concomitant gravitational instabilities within the forming allochthons resulted in the deposition of the Sedimentary Breccias Unit (SBU), which was in turn affected by albitization and quartz precipitation (Fig. 13).

7. CONCLUSION

Based on multidisciplinary dataset (rock textures, T_h of fluid inclusions, O/Sr/U-Pb isotopes), we demonstrated the occurrence of an interconnected tectonic and fluid activity under HT conditions at the former Pyrenean hyperextended domain during its extensional evolution. Hydrothermal fluids led to significant post-depositional modification of the host rocks as: diffused hydrofracturation, hydraulic brecciation, veining, recrystallization and mylonitization. New U-Pb ages on such fluid-related products strongly constrain the field and petrographic observations, which already bind the fluid activity to the whole rifting and hyperextension history. The characteristics of fluids shown in this work perfectly fit those proposed for other magma-poor rifted margins and fall in a frame that starts to be well-established in which carbonate-rich fluids evolve into silica-rich ones when the deformation starts to be accommodated by long offset extensional detachment faults. Our dataset points to a strong interaction among seawater, basement rocks and evaporites, as isotopic data suggest, at the time when

active exhumation occurred. The new discovery of authigenic albite as well as metamorphic rocks confirms that the HT-LP Pyrenean metamorphism and fluid circulation also occurred in this sector of the Western Pyrenees.

CAPTIONS

FIGURE 1 - (a) Map of the rift domains preserved in the Bay of Biscay and their fossil analogues from the Pyrenean domain. Modified after Tugend et al. (2014). (b) Restored section of the N-S transect shown in (a) across the western Pyrenees at Santonian. The study area (Chaînons Béarnais) is highlighted. Modified after Teixell et al. (2016).

FIGURE 2 - (a) Simplified geological map of the North Pyrenean Zone (NPZ). (b) Isometamorphic map of the NPZ. The Chaînons Béarnais are shown within the red circle. Modified after Clerc et al. (2015).

FIGURE 3 - (a) Simplified geological map of the Chaînons Béarnais cropping out in the easternmost part of the Mauléon basin (map modified after the BRGM 1/50,000 geological map sheets of Oloron-Ste-Marie and Lourdes). (b) Detail of the geological map of the *Lourdes map sheet* BRGM 1/50.000 showing the study area (black square in "a"), the lithostratigraphic units adopted by Casteras et al. (1970) and those used in this paper. The location of the main fluid-related products is also shown (see text for further details).

FIGURE 4 - Black Dolomites Unit (BDU). Crackle breccia: (a) TL and (b) CL images highlighting the diffuse vein sets developed along crystal contacts and within them, cemented by orange luminescing dolomite. The host rock (BDU) is dull in CL. Mosaic to rubble breccias: (c) Hand specimen; (d) CL image showing the two generations of dolomite cementing the breccias. The dolomite clasts are dull in CL; (e) TL photomicrograph of a polygenic breccia showing the relationship among the clasts, the internal dolomitized sediment and the dolomite cement; (f) crossed polarizers detail of (e).

FIGURE 5 - Black Limestones Unit (BLU). (a) TL and (b) crossed polarizers images of the "sandwiches" within the limestones. The inner part, made of Mg-rich alumo-silicates, is encased within perpendicularly growing, fibrous calcite.

FIGURE 6 - Black Limestones Unit (BLU). Type 1 breccia: (a) Field occurrence of the mosaic to rubble breccia and (b) crossed polarizers images of the cm-large clasts and the calcite cement. Type 2 breccia: (c) Field image and (d) CL images of non-luminescing dolomite clasts of Black Dolomites Unit cemented by the dark orange calcite cement. Type 3 breccia: (e) Field image and (f) TL images of the polimict clasts (limestones and dolostones) of the breccia cemented by dolomite and calcite.

FIGURE 7 - Black Limestones Unit (BLU). Mylonies and marbles: (a) Field image and (b) hand specimen of carbonate mylonites. In the bluish layers porphyroclasts of the former coarse-grained rock (marble) are preserved; (c) TL image of a porphyroblast of scapolite poikilotopically grew over the mylonitic foliation; (d) crossed polarizers image of authigenic quartz, poikilotopikally including the carbonate matrix; (e) TL and (f) CL images of white marble made up of equant, up to 500 µm-large, dolomite crystals.

FIGURE 8 - Sedimentary Breccias Unit (SBU). (a) TL image of polimict breccia. The carbonate clasts contain dolomite veins. (b) TL and (c) crossed polarizers images of polimict breccia made of carbonate clasts, with dolomite veins preserved, and larger ophite clasts. (d) TL detail of authigenic quartz poikilotopikally including carbonate crystals within the matrix of the breccias (e) TL and (f) crossed polarizers images of authigenic, randomly oriented, albite crystals grown within carbonate clasts and over the clast-matrix boundaries.

FIGURE 9 - Paragenetic sequence showing the relative timing of post-depositional processes and fluid-related products affecting the pre- to syn-tectonic sediments of the Pyrenean hyper-extended rift system. The width of the lines is qualitatively proportional to the magnitude of each process.

FIGURE 10 - (a) Histogram of the homogenization temperatures of primary fluid inclusions measured on different mineral phases of the Black Dolomites and Black Limestones Units (BDU and BLU respectively). (b) Stable isotope data: $\delta^{18}O$ versus $\delta^{13}C$ cross plot for dolomite and calcite minerals from the BDU and BLU. Measures have been accomplished on both BDU-BLU host carbonates and void filling minerals cementing hydraulic breccias. Values are given relative to VPDB standard. (c) Stable isotope results for both replacement mineral phases and void-filling cements from this study, the Adriatic distal margin (Incerpi et al. 2019) and the Galicia distal margin (Boillot et al. 1988) are also schematically compared .

FIGURE 11 - U-Pb ages obtained from the analysed samples: dolomite cements of hydraulic breccias, mylonites and host Jurassic carbonates. Time scale modified after Cohen et al. (2013; updated).

FIGURE 12 - Tera-Wasserburg diagrams for the analyzed carbonates: (a) host Black Dolomites (b) host Black Limestones; (c-d) dolomite void-filling cement of hydraulic breccias; (e-f) mylonite.

FIGURE 13 - Schematic restoration of (a) the Pyrenean rift system and (b) the study area at post-HE time. Colored dots in (b) highlight the original stratigraphic location of the rocks described in the text and shown in the colored rectangles.

TABLE 1 - O-C, Sr, T_h and U-Pb isotopic data of the analyzed samples belonging to the study area.

REFERENCES

Anderson TF and Arthur MA (1983) Stable isotopes of oxygen and carbon and their application to sedimentologic and paleoenvironmental problems. In: Arthur, M.A., Anderson, T.F., Kaplan, I.R., Veizer, J., Land, L.S., eds., Stable isotopes in sedimentary geology, 10, Columbia, SEPM Short Course, 1-151.

Asti R, Lagabrielle Y, Fourcade S, Corre B, Monié P (2019) How do continents deform during mantle exhumation? Insights from the northern Iberia inverted paleopassive margin, Western Pyrenees (France). Tectonics, 38. https://doi.org/10.1029/2018TC005428.

Azambre B, Rossy M, Albarède F (1992) Petrology of the alkaline magmatism from the Cretaceous North-Pyrenean rift zone (France and Spain). European Journal of Mineralogy, 4, 813-834.

Azambre B, Rossy M, Lago M (1987) Caractéristiques pétrologiques des dolérites tholéitiques d'âge triasiques (ophites) du domaine pyrénéen. B. Mineral., 110: 379-96.

Bayrakci G, Minshull TA, Sawyer DS, Reston TJ, Klaeschen D, Papenberg C, Ranero C, Bull JM, Davy RG, Shillington DJ, Perez-Gussinye M, Morgan JK (2016) Fault-controlled hydration of the upper mantle during continental rifting. Nature Geoscience Letters, DOI: 10.1038/NGEO2671

Beltrando M, Manatschal G, Mohn G, Dal Piaz GV, Vitale Brovarone A, Masini E (2014) Recognizing remnants of magma-poor rifted margins in high-pressure orogenic belts: The Alpine case study. Earth-Science Reviews, 131: 88-115.

Boillot G, Winterer EL, Meyer AW (1988) *Proceedings of the Ocean Drilling Program, 103 Initial Reports*, Proceedings of the Ocean Drilling Program, edited by G. Boillot, E. L. Winterer, and A. W. Meyer, Ocean Drilling Program.

Boschi C, Früh-Green L, Delacour A, Karson JA, Kelley DS (2006) Mass transfer and fluid flow during detachment faulting and develepoment of an oceanic core complex, Atlantis Massif (MAR 30°N). Geochemistry, Geophysics, Geosystems, 7, Q01004, doi:10.1029/2005GC001074.

Boulvais P, Ruffet G, Cornichet J, Mermet M. (2007) Cretaceous albitization and dequartzification of Hercynian peraluminous granite in the Salvezines Massif (French Pyrenees). Lithos, 93:89-106.

Boulvais P, de Parseval P, D'Hulst A, Paris P (2006) Carbonate alteration associated with talc-chlorite mineralization in the eastern Pyrenees, with emphasis on the St. Barthelemy Massif. Mineralogy and Petrology, 88:499-526.

Breitenbach SFM and Bernasconi SM (2011) Carbon and oxygen isotope analysis of small carbonate samples (20 to 100 μg) with a GasBench II preparation device. Rapid Communications in Mass Spectrometry, 25: 1910–1914.

Brune S, Heine C, Perez-Gussinye M, Sobolev SV (2014) Rift migration explains continental margin asymmetry and crustal hyper-extension. Nature Communications, 5: 4014. DOI: 10.1038/ncomms5014

Castanares LM, Robles S, Gimeno D, Vicente Bravo JC (2001) The Submarine Volcanic System of the Errigoiti Formation (Albian-Santonian of the Basque-Cantabrian Basin, Northern Spain): Stratigraphic Framework, Facies, and Sequences. Journal of Sedimentary Research, 71: 318-333, doi:10.1306/080700710318.

Castanares LM, Robles S, Vicente Bravo JC (1997) Distribution estratigrafica de los episodios volcanicos submarinos del Albiense-Santoniense en la Cuenca Vasca (sector Gernika-Plentzia, Bizkaia). Geogaceta, 22: 43-46.

Casteras M, Godechot Y, Villanova M (1970) Feuille de Lourdes (1052), Carte géologique de la France 1/50,000. Bureau de Recherche Géologique et Minières, Orléans, France.

Claude D (1990). Etude stratigraphique, sédimentologique et structural des dépôts mésozoïques au Nord du massif du Labourd. Rôle de la faille de Pamplona (Pays Basque). PhD thesis, Université de Bordeaux III, pp. 252.

Clerc C, Lahfid A, Monié P, Lagabrielle Y, Chopin C, Pujol M, Boulvais P, Ringenbach JC, Masini E, de St Blanquat M (2015) High-temperature metamorphism during extreme thinning of the continental crust: a reappraisal of the North Pyrenean passive paleomargin. Solid Earth, 6: 643-668.

Clerc C and Lagabrielle Y (2014) Thermal control on the modes of crustal thinning leading to mantle exhumation. Insights from the Cretaceous Pyrenean hot paleomargins, Tectonics, 33:1340-1359, doi:10.1002/2013TC003471.

Clerc C, Lagabrielle Y, Neumaier M, Reynaud J-Y, de Saint Blanquat M (2012) Exhumation of subcontinental mantle rocks: evidence from ultramafic-bearing clastic deposits nearby the Lherz peridotite body, French Pyrenees. Bulletin de la Société Géologique de France, 183(5):443-459.

Cohen KM, Finney SC, Gibbard PL, Fan JX (2013; updated) The ICS International Chronostratigraphic Chart. Episodes, 36: 199–204.

Coltat R, Boulvais P, Branquet Y, Collot J, Epin ME, Manatschal G (2019) Syntectonic carbonation during synmagmatic mantle exhumation at an ocean-continent transition. Geology, 47: 183-186. https://doi.org/10.1130/G45530.1.

Corre B, Boulvais P, Boiron MC, Lagabrielle Y, Marasi L, Clerc C (2018) Fluid circulations in response to mantle exhumation at the passive margin setting in the north Pyrenean zone, France. Mineralogy and Petrology, https://doi.org/10.1007/s00710-018-0559-x

DeFelipe I, Pedreira D, Pulgar JA, Iriarte E, Mendia M (2017) Mantle exhumation and metamorphism in the Basque-Cantabrian Basin (N Spain): Stable and clumped isotope analysis in carbonates and comparison with ophicalcites in the North-Pyrenean Zone (Urdach and Lherz). Geochemistry, Geophysics, Geosystems, 18, doi:10.1002/2016GC006690.

Ducasse L, Vélasque P (1986) Glissement de couverture et panneaux basculés dans la région des Arbailles (Pyrénées occidentales): un modèle évolution crétacé de la marge nord-ibérique à l'Est de la transformante de Pamplona. Compte Rendu de l'Académie des Sciences, 303(16):1477-1482.

Epin ME, Manatschal G, Amann, M (2017) Defining diagnostic criteria to describe the role of the rift inheritance in collisional orogens: The case of the Err-Platta nappes (Switzerland). Swiss Journal of Geosciences, 110: 419–438.

Fallourd S, Poujol M, Boulvais P, Paquette J-L, de Saint Blanquat M, Remy P (2014) In situ LA-ICP-MS U–Pb titanite dating of Na–Ca metasomatism in orogenic belts: the North Pyrenean example. International Journal of Earth Science. 103:667-682.

Filleaudeau PY, Mouthereau F, Pik R (2012) Thermo-tectonic evolution of the south-central Pyrenees from rifting to orogeny: insights from detrital zircon U/Pb and (U-Th)/He thermochronometry. Basin Research, 24:401-417.

Garcìa-Senz J, Pedrera A, Ayala C, Ruiz-Constan A, Robador A, Rodriguez-Fernandez LR (2019) Inversion of the north Iberian hyperextended margin: the role of exhumed mantle indentation during continental collision. In: Hammerstein JA, Di Cuia R, Cottam MA, Zamora G, Butler RWH (eds) Fold and Thrust Belts: Structural Style,

Evolution and Exploration. Geological Society, London, Special Publications, 490, https://doi.org/10.1144/SP490-2019-112

Gerdes A and Zeh A (2006) Combined U-Pb and Hf isotope LA-(MC-)ICP-MS analyses of detrital zircons: Comparison with SHRIMP and new constraints for the provenance and age of an Armorican metasediment in Central Germany. Earth and Planetary Science Letters, 249: 47-62. https ://doi.org/10.1016/j.epsl.2006.06.039

Gerdes A and Zeh A (2009) Zircon formation versus zircon alteration-New insights from combined U-Pb and Lu-Hf in-situ La-ICP-MS analyses of Archean zircons from the Limpopo Belt. Chemical Geology, 261(3–4): 230-243.

Golberg JM, Maluski H, Leyreloup AF (1986) Petrological and age relationship between emplacement of magmatic breccia, alkaline magmatism, and static metamorphism in the North Pyrenean Zone. Tectonophysics, 129(1–4): 275-290, doi:10.1016/0040-1951(86)90256-8.

Haeri-Ardakani O, Al-Aasm I, Coniglio M (2013) Fracture mineralization and fluid flow evolution: an example from Ordovician-Devonian carbonates, southwestern Ontario, Canada. Geofluids, 13:1-20.

Hart NR, Stockli DF, Lavier LL, Hayman NW (2017) Thermal evolution of a hyper-extended rift basin, Mauleon Basin, Western Pyrenees. Tectonics, 36: 1103-1128. https ://doi.org/10.1002/2016T C004365

Henry P, Azambre B, Montigny R, Rossy M, Stevenson RK (1998) Late mantle evolution of the Pyrenean sub-continental lithospheric mantle in the light of new 40Ar-39Ar and Sm-Nd ages on pyroxenites and peridotites (Pyrenees, France). Tectonophysics, 296(1-2): 103-123, doi:10.1016/S0040-1951(98)00139-5.

Hensen C, Duarte JC, Vannucchi P, Mazzini A, Lever MA, Terrinha P, Géli L, Henry P, Villinger H, Morgan J, Schmidt M, Gutscher MA, Bartolome R, Zomonaga Y, Polonia A, Gràcia E, Tinivella U, Lupi M, Çagatay MN, Elvert M, Sakellariou D, Matias L, Kipfer R, Karageorgis AP, Ruffine L, Liebetrau V, Pierre C, Schmidt C, Batista L, Gasperini L, Burwicz E, Neres M, Nuzzo M (2019) Marine transform faults and fracture zones: a joint perspective integrating seismicity, fluid flow and life. Frontiers in Earth Sciences, 7:39, doi: 10.3389/feart.2019.00039.

Hensen C, Nuzzo M, Hornibrook E, Pinheiro L, Bock B, Magalhaes V, Bruckmann W (2007) Sources of mud volcano fluids in the Gulf of Cadiz-indications for hydrothermal imprint. Geochimica et Cosmochimica Acta, 71:1232-1248.

Hollis C, Bastesen E, Boyce A, Corlett H, Gawthorpe R, Hirani J, Rotevatn A, Whitaker F (2017) Fault-controlled dolomitization in a rift basin. Geology, 45: 219-222.

Horita J (2014) Oxygen and carbon isotope fractionation in the system dolomite-water-CO_2 to elevated temperatures. Geochimica et Cosmochimica Acta, 129:111-124.

Incerpi N, Martire L, Manatschal G, Bernasconi SM, Gerdes A, Czuppon G, Palcsu L, Karner GD, Johnson CA, Figueredo PH (2019) Hydrothermal fluid flow associated to the extensional evolution of the Adriatic rifted margin: Insights from the pre- to post-rift sedimentary sequence (SE Switzerland, N Italy). Basin Research, DOI: 10.1111/bre.12370.

Incerpi N, Martire L, Bernasconi SM, Manatschal G, Gerdes A (2018) Silica-rich septarian concretions in biogenic silica-poor sediments: A marker of hydrothermal activity at fossil hyper-extended rifted margins (Err nappe, Switzerland). Sedimentary Geology, 378: 19-33. https ://doi.org/10.1016/j.sedgeo.2018.10.005

Incerpi N, Martire L, Manatschal G, Bernasconi S (2017) Evidence of hydrothermal fluid flow in a hyperextended rifted margin: the case study of the Err nappe (SE Switzerland). Swiss Journal of Geosciences. DOI: 10.1007/s00015-016-0235-2.

Jammes S, Lavier LL, Manatschal G (2010a) Extreme crustal thinning in the Bay of Biscay and the Western Pyrenees: from observations to modeling. Geochemistry, Geophysics, Geosystems, DOI: 10.1029/2010GC003218.

Jammes S, Manatschal G, Lavier LL (2010b) Interaction between prerift salt and detachment faulting in hyperextended rift systems: the example of the Parentis and Mauléon basins (Bay of Biscay and western Pyrenees). American Association of Petroleum Geologist Bulletin, 94(7): 957-975.

Jammes S, Manatschal G, Lavier L, Masini E (2009) Tectono-sedimentary evolution related to extreme crustal thinning ahead of a propagating ocean; example of the western Pyrenees. Tectonics, DOI: 10.1029/2008TC002406.

Johnson JA and Hall CA (1989a) The structural and sedimentary evolution of the Cretaceous North Pyrenean Basin, southern France. Geological Society of America Bulletin, 101:231-247.

Johnson JA and Hall CA (1989b) Tectono-stratigraphic model for the massif d'Igountze-Mendibelza, western Pyrenees. Journal of the Geological Society of London, 146:925-932.

Kastner M (1971) Authigenic feldspars in carbonate rocks. American Mineralogy, 56:1403-1442.

Lagabrielle Y, Clerc C, Vauchez A, Lahfid A, Labaume P, Azambre B, Fourcade S, Dautria JM (2016) Very high geothermal gradient during mantle exhumation recorded in mylonitic marbles and carbonate breccias from a Mesozoic Pyrenean palaeomargin (Lherz area, North Pyrenean Zone, France). Comptes Rendus Geoscience, 348: 290-300.

Lagabrielle Y, Labaume P, De Saint Blanquat M (2010) Mantle exhumation, crustal denudation, and gravity tectonics during Cretaceous rifting in the Pyrenean realm (SW Europe): insights from the geological setting of the lherzolite bodies. Tectonics, 29 (TC4012).

Lagabrielle Y and Bodinier JL (2008) Submarine reworking of exhumed subcontinental mantle rocks; field evidence from the Lherz peridotites, French Pyrenees. Terra Nova, 20(1):11-21.

Land LS (1985) The origin of massive dolomite. Journal of Geological Education, 33, 112–125. https ://doi.org/10.5408/0022-1368-33.2.112

Lescoutre R, Tugend J, Brune S, Masini E, Manatschal G (2019) Thermal evolution of asymmetric magma-poor rift systems: results from numerical modeling and Pyrenena field observations. Geochemistry, Geophysics, Geosystems, https://doi.org/10.1029/2019GC008600

López-Horgue MA, Owen HG, Aranburu A, Fernandez-Mendiola PA, Garcia-Mondéjar J (2009) Early late Albian (Cretaceous) of the central region of the Basque-Cantabrian Basin, northern Spain: biostratigraphy based on ammonites and orbitolinids. Cretaceous Research, 30: 385-400, doi:10.1016/j.cretres.2008.08.001.

López-Horgue MA, Owen HG, Rodriguez-Lázaro J, Orue-Etxebarria, Fernández-Mendiola PA, Garcıa-Mondéjar J (1999) Late Albian–Early Cenomanian stratigraphic succession near Estella-Lizarra (Navarra, central northern Spain) and its regional and interregional correlation, Cretaceous Research, 20: 369-402, doi:10.1006/cres.1999.0162.

Machel HG (2004) Concepts and models of dolomitization: a critical reappraisal. In Braithwaite, C. J. R., Rizzi, G., & Darke, G. (Eds.), The geometry and petrogenesis of dolomite hydrocarbon reservoirs. Geological Society, London, Special Publications, 235(1): 7-63.

Masini E, Manatschal G, Tugend J, Mohn G, Flament JM (2014) The tectono-sedimentary evolution of a hyper-extended rift basin: the example of the Arzacq–Mauléon rift system (Western Pyrenees, SW France). International Journal of Earth Sciences, DOI 10.1007/s00531-014-1023-8.

Masini E, Manatschal G, Mohn G, Ghienne J F, Lafont F (2011) The tectono-sedimentary evolution of a supra-detachment rift basin at a deep-water magma-poor rifted margin: The example of the Samedan Basin preserved in the Err nappe in SE Switzerland. Basin Research, 23: 652-677. https ://doi.org/10.1111/j.1365-2117.2011.00509.x

McArthur JM, Howarth RJ, Shields GA (2012) Strontium Isotope Stratigraphy. In: Gradstein F.M., Ogg JG, Schmitz M, Ogg G (Eds.), The Geologic Time Scale 2012:127-144, Elsevier.

McKenzie JA (1991) The dolomite problem: An outstanding controversy. In Muller DW, McKenzie JA, Weissert H (Eds.), Controversies in modern geology: Evolution of geological theories in sedimentology (pp. 37–54). London, UK: Academic Press.

Meister P, Mckenzie JA, Bernasconi SM (2013) Dolomite formation in the shallow seas of the Alpine Triassic. Sedimentology, 60:270-291.

Montigny R, Azambre B, Rossy M, Thuizat R (1986) K-Ar study of Cretaceous magmatism and metamorphism from Pyrenees; age and length of rotation of the iberian peninsula. Tectonophysics, 129:257-274.

Montigny R, Azambre B, Rossy M, Thuizat R (1982) Etude K/Ar du magmatisme basique lié au Trias supérieur des Pyrénées - Conséquences méthodologiques et pétrographiques, B. Mineral., 105: 673-680.

Morrow DW (1982) Descriptive field classification of sedimentary and diagenetic breccias fabrics in carbonate rocks. Bulletin of Canadian Petroleum Geology, 30:227-229.

Mouthereau F, Filleaudeau PY, Vacherat A, Pik R, Lacombe O, Fellin MG, Castelltort S, Christophoul F, Masini E (2014) Placing limits to shortening evolution in the Pyrenees: role of margin architecture and implications for the Iberia/Europe convergence. Tectonics, 33:2283-2314.

Pedreira D, Pulgar JA, Gallart J, Torné M (2007) Three-dimensional gravity and magnetic modeling of crustal indentation and wedging in the western Pyrenees–Cantabrian Mountains. Journal of Geophysical Research, 112. doi:10.1029/2007JB005021.

Picazo S, Lafay R, Faucheux V, Vennemann T (2019) New constraints on carbonation associated with brecciation in hyper-extended margins (example of Iberia and Newfoundland margins). Terra Nova, https://doi.org/10.1111/ter.12383

Pinto VH, Mnatschal G, Karpoff AM, Ulrich M, Viana AR (2016) Seawater storage and element transfer associated with mantle serpentinization in magma-poor rifted margins: a quantitative approach. Earth and Planetary Science Letters, http://dx.doi.org/10.1016/j.epsl.2016.11.023

Pinto VH, Manatschal G, Karpoff AM, Viana A (2015) Tracing mantle-reacted fluids in magma-poor rifted margin: The example of Alpine Tethyan rifted margin. Geochemistry, Geophysics, Geosystems, 16:3271-3308.

Poujol M, Boulvais P, Kosler J (2010) In-situ LA–ICP–MS U–Th–Pb dating of metasomatic fluid circulation: Evidence of regional-scale albitization in the Pyrenees. Journal of the Geological Society, 167:751-767.

Purser BH, Tucker ME, Zenger DH (1994) Dolomites - A volume in honour of Dolomieu. International Association of Sedimentologists, Special Publications, 21.

Quesnel B, Boiron MC, Cathelineau M, Truche L, Rigaudier T, Bardoux G, Agrinier P, de St Blanquat M, Masini E, Gaucher EC (2019) Nature and origin of mineralizing fluids in hyperextensional systems: The case of cretaceous Mg metasomatism in the Pyrenees. Geofluids, https://doi.org/10.1155/2019/7213050

Rais P, Louis-Schmid B, Bernasconi SM, Reusser E, Weissert H (2008) Distribution of authigenic albites in a limestone succession of the Helvetic Domain, eastern Switzerland. Swiss Journal of Geosciences, 101:99-106.

Renard S, Pironon J, Sterpenich J, Carpentier C, Lescanne M, Gaucher EC (2019) Diagenesis in Mesozoic carbonate rocks in the North Pyrenees (France) from mineralogy and fluid inclusion analysis: Example of Rousse reservoir and caprock. Chemical Geology, 508: 30-46. https ://doi.org/10.1016/j.chemg eo.2018.06.017

Ribes C, Manatschal G, Ghienne JF, Karner GD, Johnson CA, Figueredo PH, Incerpi N, Epin ME (2019a) The syn-rift stratigraphic record across a fossil hyper-extended rifted margin: the example of the northwestern Adriatic

margin exposed in the Central Alps. International Journal of Earth Sciences, https://doi.org/10.1007/s00531-019-01750-6

Ribes C, Ghienne JF, Manatschal G, Decarlis A, Karner GD, Figueredo PH, Johnson CA (2019b) Long-lived mega fault-scarps and related breccias at distal rifted margins: Insights from present-day and fossil analogues. Journal of the Geological Society, DOI: https://doi.org/10.1144/jgs2018-181

Richter DK, Götte T, Habermann D (2002) Cathodoluminescence of authigenic albite. Sedimentary Geology, 150:367-374.

Roca E, Muñoz JA, Ferrer O, Ellouz N (2011) The role of the Bay of Biscay Mesozoic extensional structure in the configuration of the Pyrenean orogen: constraints from the MARCONI deep seismic reflection survey. Tectonics, 30 (TC2001).

Rossy M, Azambre B, Albarède F (1992) REE and Sr/1bNd isotope geochemistry of the alkaline magmatism from the Cretaceous North Pyrenean Rift Zone (France-Spain), Chemical Geology, 97: 33-46, doi:10.1016/0009-2541(92)90134-Q.

Rossy M (1988) Contribution à l'étude du magmatisme mésozoïque du domaine Pyrénéen, I, Le Trias dans l'ensemble du domaine; II, Le Crétacé dans les provinces Basques d'Espagne, Thèse, Université de Besançon, Besançon.

Salardon R, Carpentier C, Bellahsen N, Pironon J, France-Lanord C (2017) Interactions between tectonics and fluid circulations in an inverted hyper-extended basin: Example of mesozoic carbonate rocks of the western North Pyrenean Zone (Chaînons Béarnais, France). Marine and Petroleoum Geology, 80:563-586.

San Miguel de la Camara M (1952) Las eruptiones y las rocas volcanicas de las Vascongadas, Munibe, 2-3: 115-130.

Saspiturry N, Razin P, Baudin T, Serrano O, Issautier B, Lasseur E, Allanic C, Thinon I, Leleu S (2019) Symmetry vs. asymmetry of a hyper-thinned rift: Example of the Mauléon Basin (Western Pyrenees, France). Marine and Petroleum Geology, 104: 86-105.

Schärer U, de Parseval P, Polvé M, de Saint Blanquat M (1999) Formation of the Trimouns talc-chlorite deposit (Pyrenees) from persistent hydrothermal activity between 112 and 97 Ma. Terra Nova, 11:30-37.

Spötl C, Longstaffe FJ, Ramseyer K, Rüdinger B (1999) Authigenic albite in carbonate rocks - a tracer fro deep-burial brine migration? Sedimentology, 46:649-666.

Sun Z, Jian Z, Stock JM, Larsen HC, Klaus A, Alvarez Zarikian CA, the Expedition 367/368 Scientists (2018a) Proceedings of the International Ocean Discovery Program. vol. 367/368. https://doi.org/10.14379/iodp.proc.367368.103.2018 (publications.iodp.org).

Sun Z, Jian Z, Stock JM, Larsen HC, Klaus A, Alvarez Zarikian CA, the Expedition 367/368 Scientists (2018b). Proceedings of the International Ocean Discovery Program. vol. 367/368. https://doi.org/10.14379/iodp.proc.367368.105.2018 (publications.iodp.org).

Teixell A, Labaume P, Lagabrielle Y (2016) The crustal evolution of the west-central Pyrenees revisited: inferences from a new kinematic scenario. Compte Rendu Geosciences, 348:257-267.

Tucker ME, Wright VP (1990) Carbonate sedimentology. Blackwell, Oxford, 428 pp.

Tugend J, Manatschal G, Kusznir NJ (2015) Spatial and temporal evolution of hyperextended rift systems: Implication for the nature, kinematics, and timing of the Iberian-European plate boundary. Geology, 43:15-18. doi: 10.1130/G36072.1

Tugend J, Manatschal G, Kusznir NJ, Masini E, Mohn G, Thinon I (2014) Formation and deformation of hyperextended rift systems: Insights from rift domain mapping in the Bay of Biscay-Pyrenees. Tectonics, 33, DOI:10.1002/2014TC003529.

Vacherat A, Mouthereau F, Pik R, Bellahsen N, Gautheron C, Bernet M, Daudet M, Balansa J, Tibari B, Pinna Jamme R, Radal J (2016) Rift-to-collision transition recorded by tectonothermal evolution of the northern Pyrenees. Tectonics, 35. doi.org/10.1002/2015TC004016.

Vacherat A, Mouthereau F, Pik R, Bernet M, Gautheron C, Masini E, Lahfid A (2014) Thermal imprint of rift-related processes in orogens as recorded in the Pyrenees. Earth and Planetary Science Letters, 408: 296-306. https ://doi.org/10.1016/j.epsl.2014.10

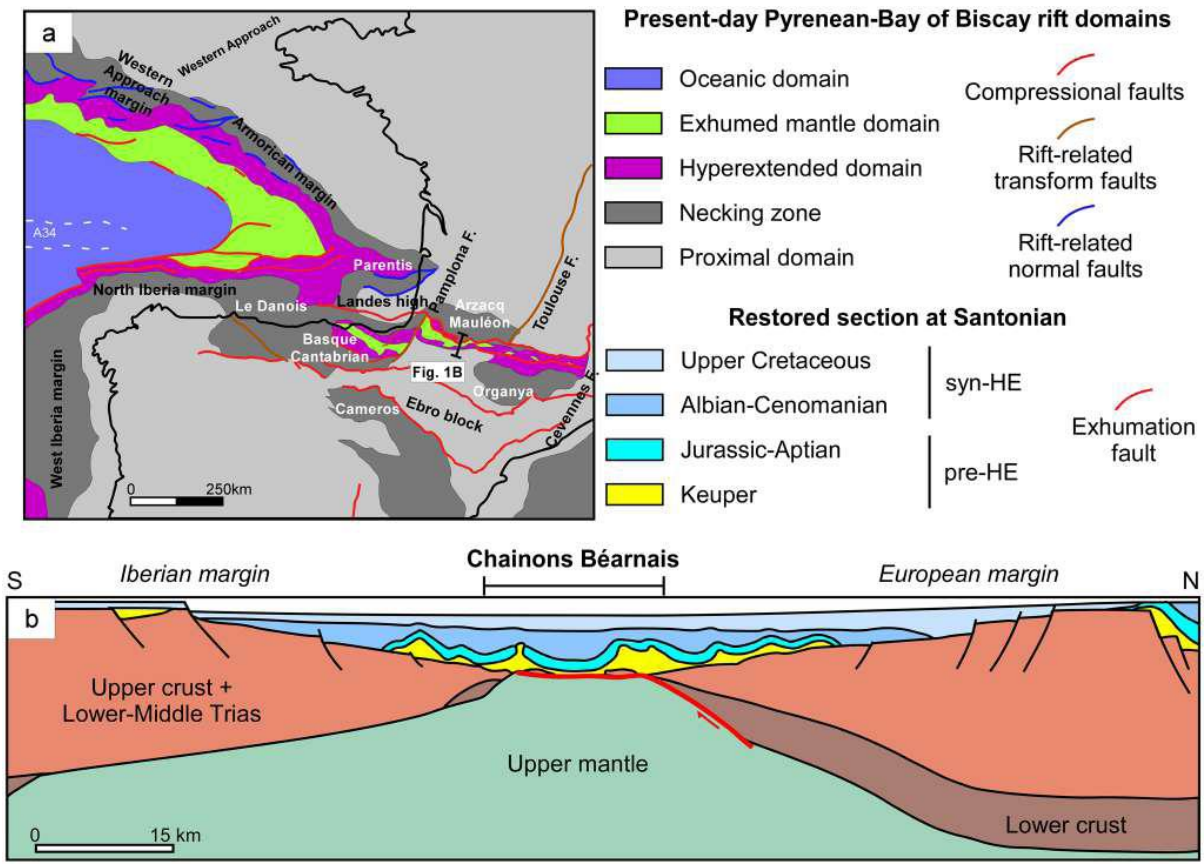
a
Western Approach
Western Approach margin
Armorican margin
A34
Parentis
North Iberia margin
Le Danois
Landes high
Pamplona F.
Arzacq
Mauléon
Toulouse F.
Basque Cantabrian
Fig. 1B
Organya
Cameros
Ebro block
Cevennes F.
West Iberia margin
0
250km
Present-day Pyrenean-Bay of Biscay rift domains
Oceanic domain
Exhumed mantle domain
Hyperextended domain
Necking zone
Proximal domain
Compressional faults
Rift-related transform faults
Rift-related normal faults
Restored section at Santonian
Upper Cretaceous
Albian-Cenomanian
Jurassic-Aptian
Keuper
syn-HE
pre-HE
Exhumation fault
S
Iberian margin
Chainons Béarnais
European margin
N
b
Upper crust + Lower-Middle Trias
Upper mantle
Lower crust
0
15 km

Fig. 1

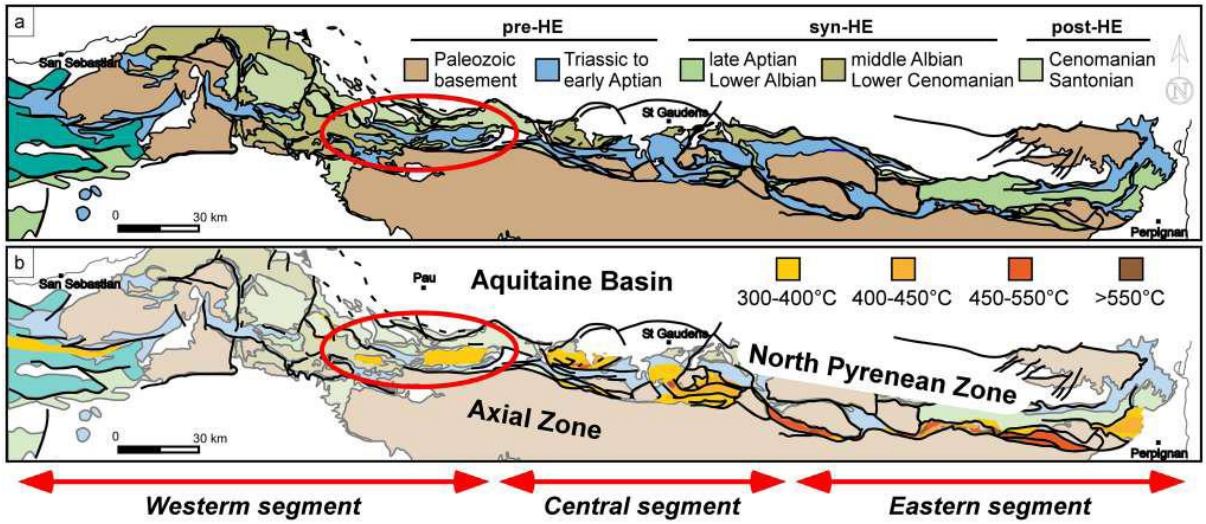
a
pre-HE
syn-HE
post-HE
Paleozoic basement
Triassic to early Aptian
late Aptian Lower Albian
middle Albian Lower Cenomanian
Cenomanian Santonian
San Sebastian
St Gaudens
0
30 km
Perpignan
b
Pau
Aquitaine Basin
300-400°C
400-450°C
450-550°C
>550°C
North Pyrenean Zone
Axial Zone
Westerm segment
Central segment
Eastern segment

Fig. 2

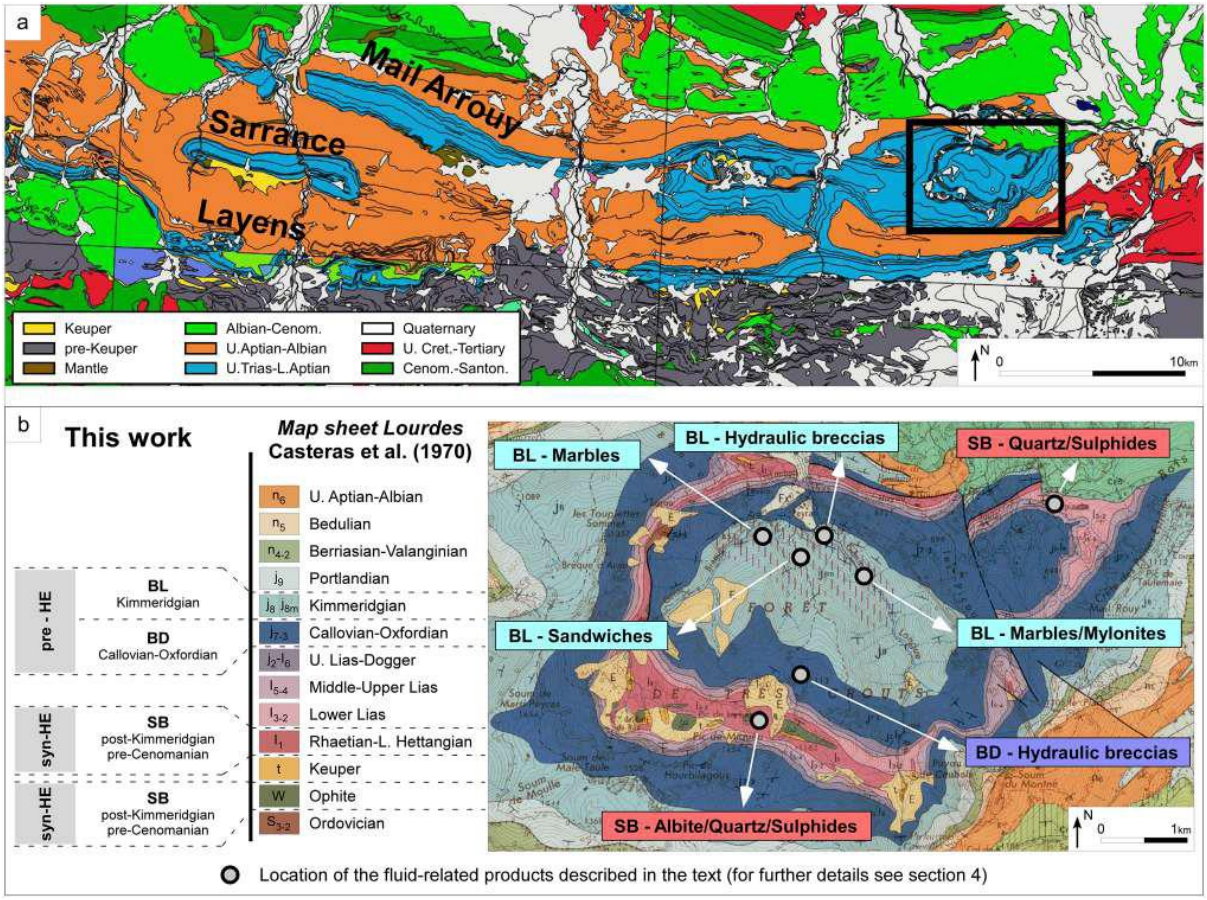
a
Mail Arrouy
Sarrance
Layens
Keuper
pre-Keuper
Mantle
Albian-Cenom.
U.Aptian-Albian
U.Trias-L.Aptian
Quaternary
U. Cret.-Tertiary
Cenom.-Santon.
N
0
10km
b
This work
Map sheet Lourdes
Casteras et al. (1970)
pre - HE
BL
Kimmeridgian
BD
Callovian-Oxfordian
syn-HE
SB
post-Kimmeridgian
pre-Cenomanian
syn-HE
SB
post-Kimmeridgian
pre-Cenomanian
U. Aptian-Albian
Bedulian
Berriasian-Valanginian
Portlandian
Kimmeridgian
Callovian-Oxfordian
U. Lias-Dogger
Middle-Upper Lias
Lower Lias
Rhaetian-L. Hettangian
Keuper
Ophite
Ordovician
BL - Marbles
BL - Hydraulic breccias
SB - Quartz/Sulphides
BL - Sandwiches
BL - Marbles/Mylonites
BD - Hydraulic breccias
SB - Albite/Quartz/Sulphides
N
0
1km
Location of the fluid-related products described in the text (for further details see section 4)

Fig. 3

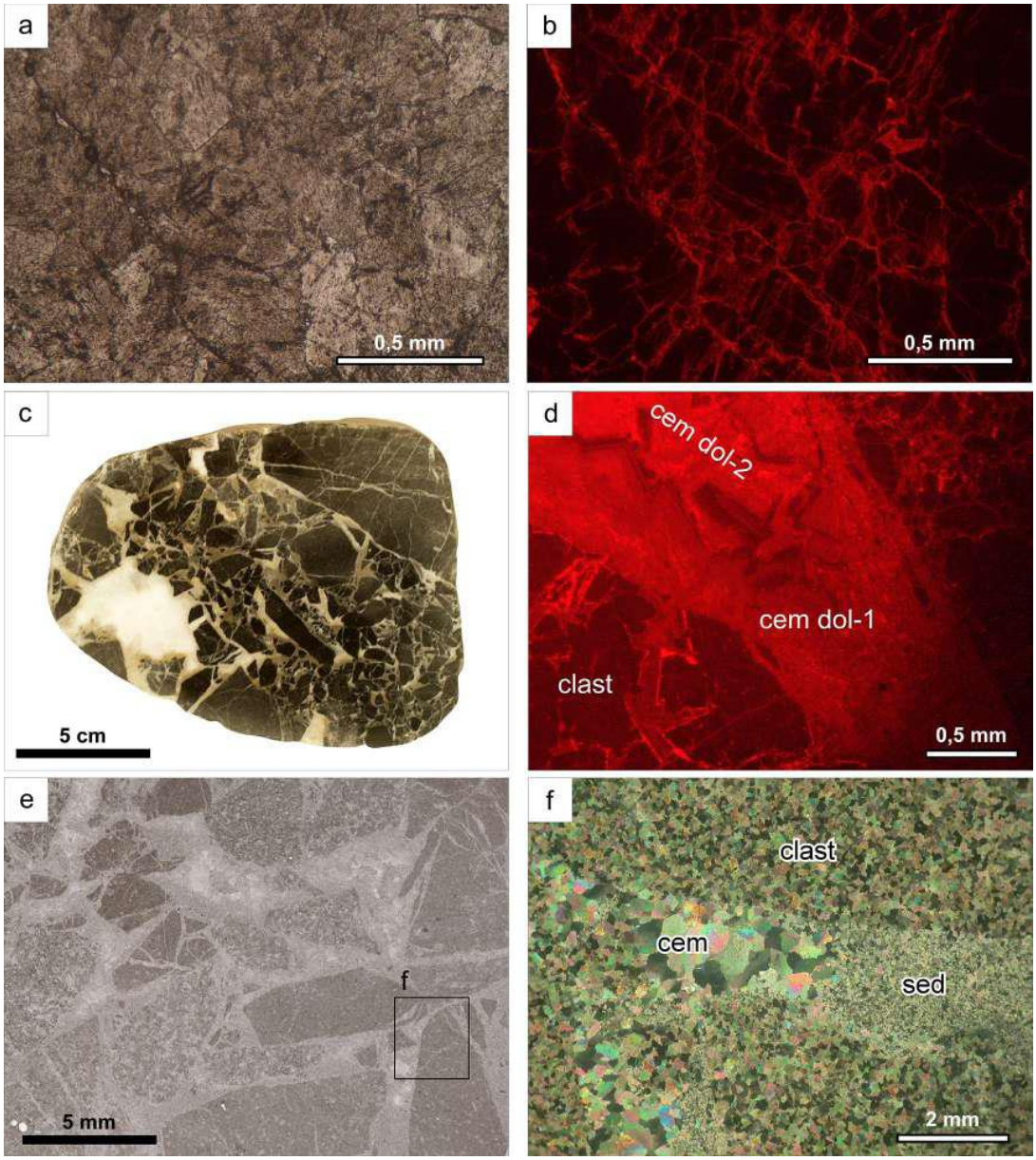
a
0,5 mm
b
0,5 mm
c
5 cm
d
cem dol-2
cem dol-1
clast
0,5 mm
e
f
5 mm
f
clast
cem
sed
2 mm

Fig. 4

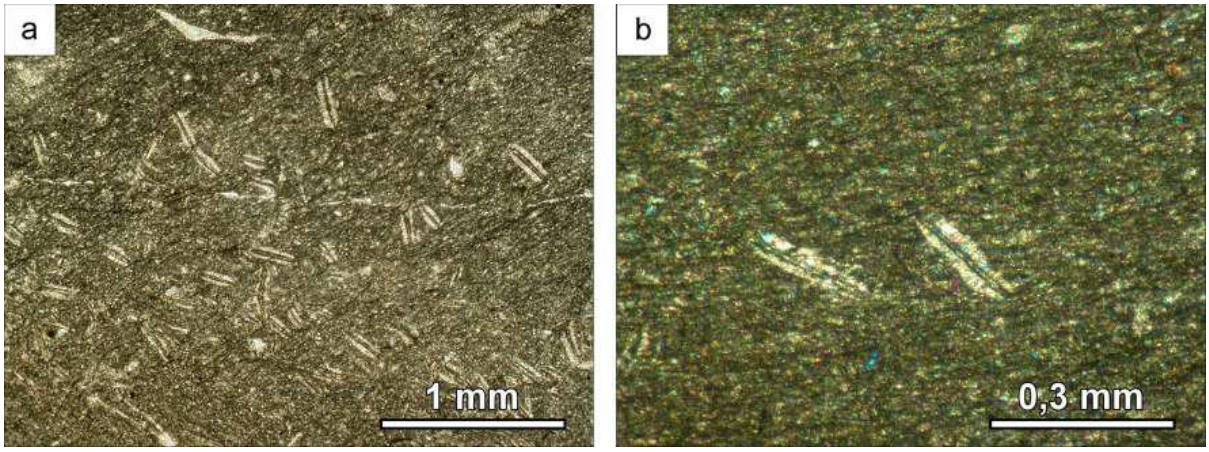

Fig. 5

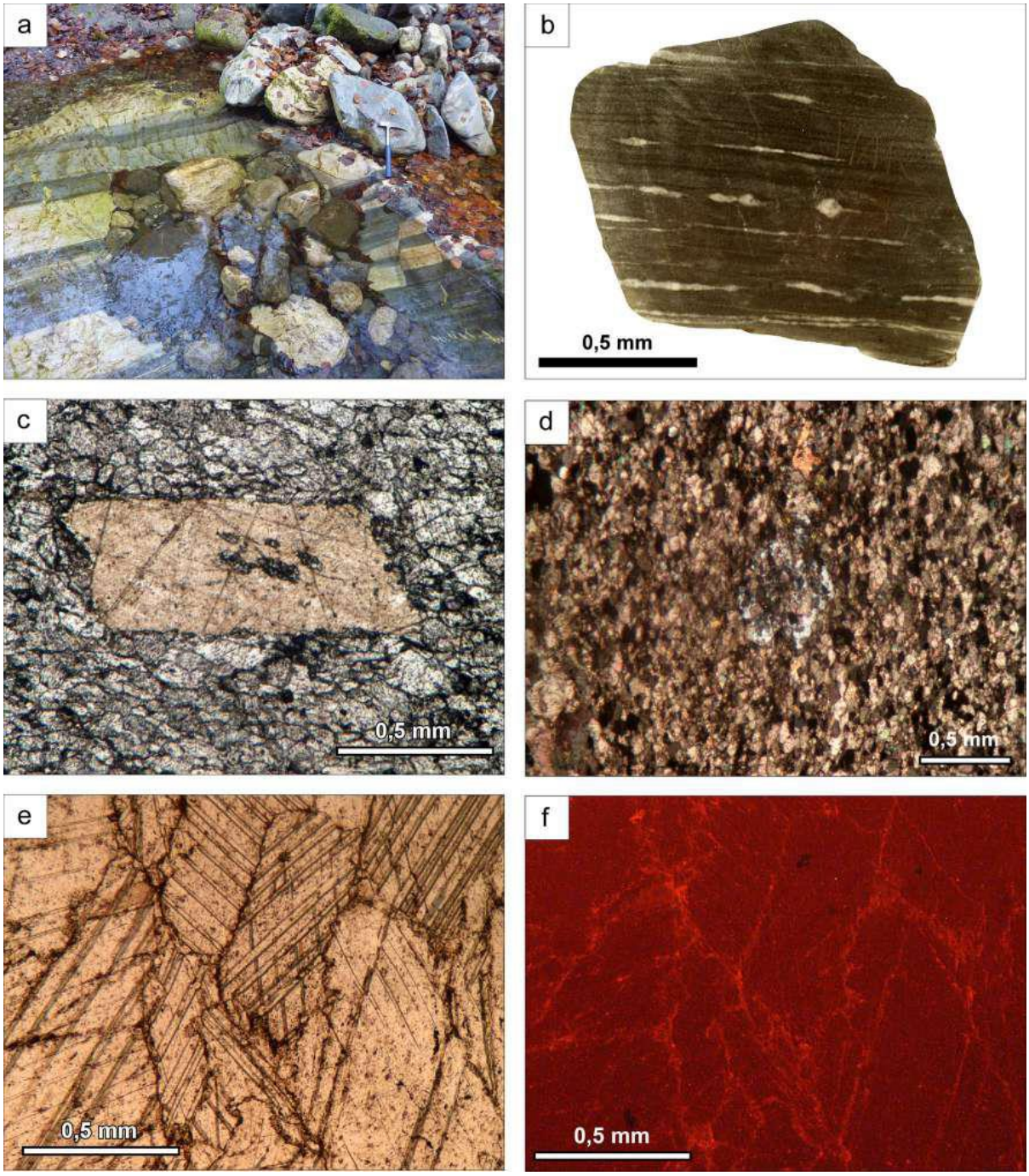

Fig. 6

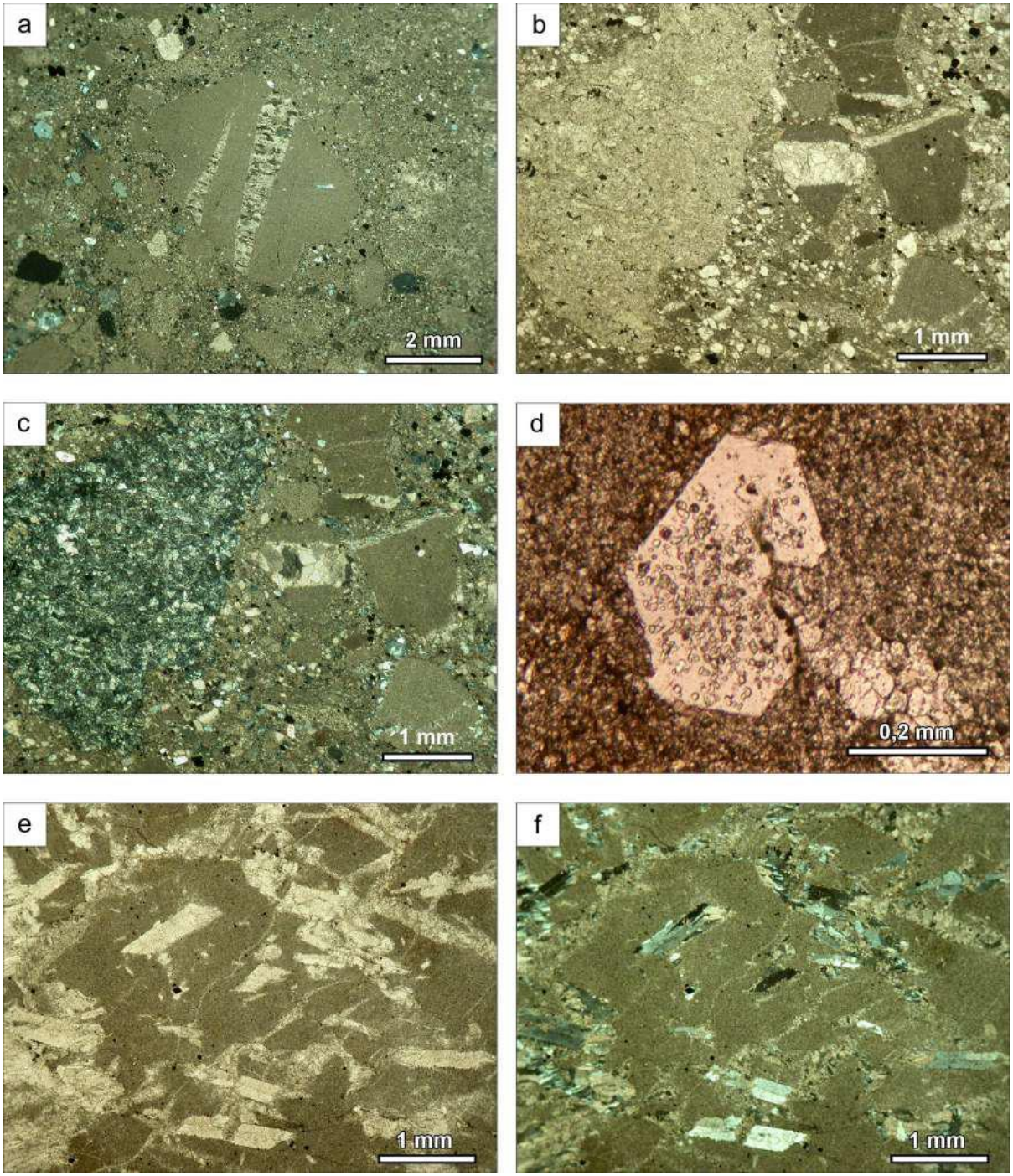

Fig. 7

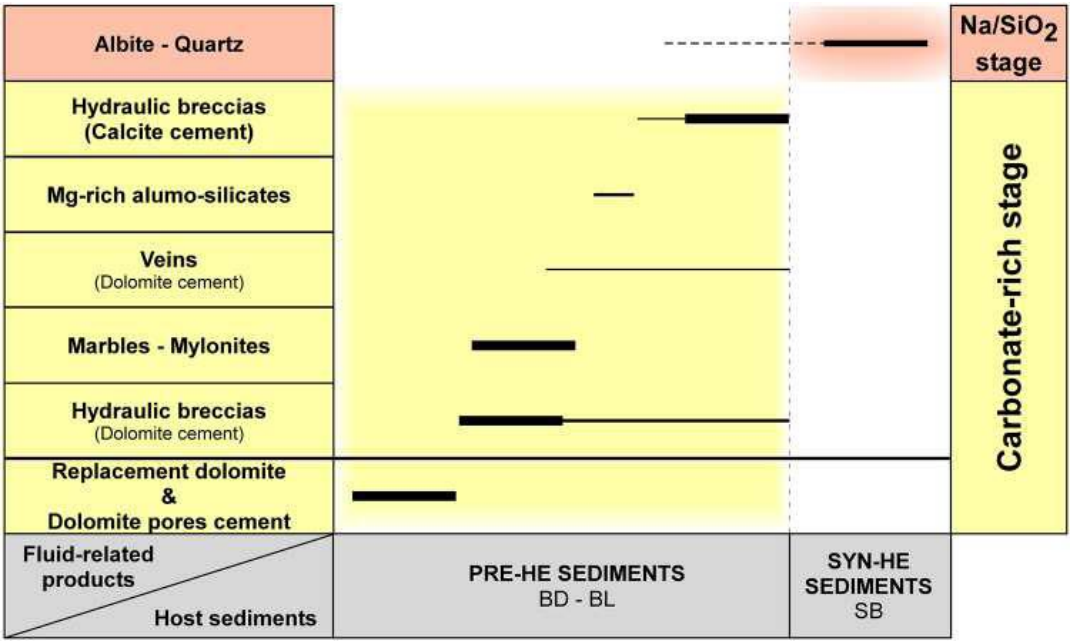
Albite - Quartz
Hydraulic breccias (Calcite cement)
Mg-rich alumo-silicates
Veins (Dolomite cement)
Marbles - Mylonites
Hydraulic breccias (Dolomite cement)
Replacement dolomite & Dolomite pores cement
Fluid-related products
Host sediments
PRE-HE SEDIMENTS BD - BL
SYN-HE SEDIMENTS SB
Na/SiO2 stage
Carbonate-rich stage

Fig. 8

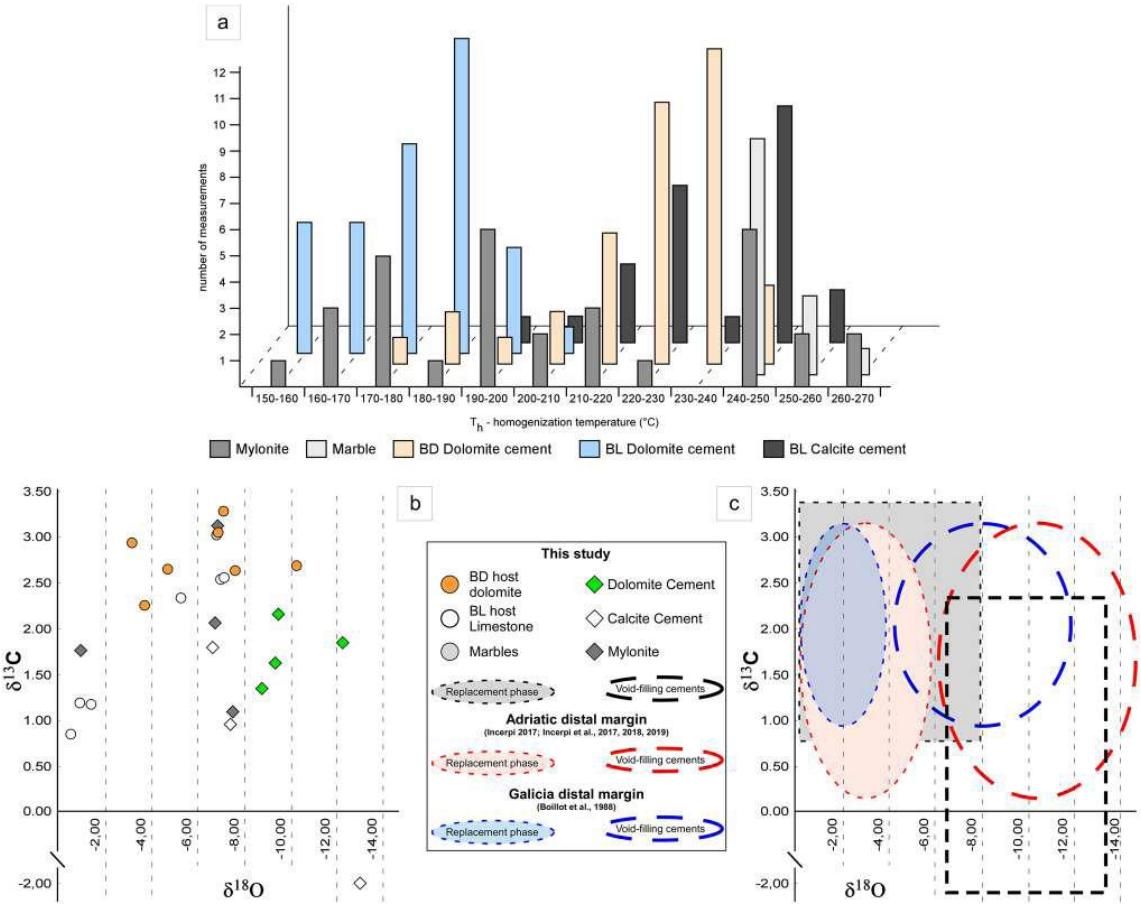
a
number of measurements
150-160
160-170
170-180
180-190
190-200
200-210
210-220
220-230
230-240
240-250
250-260
260-270
Th - homogenization temperature (°C)
Mylonite
Marble
BD Dolomite cement
BL Dolomite cement
BL Calcite cement
b
c
δ13C
δ18O
This study
BD host dolomite
BL host Limestone
Marbles
Dolomite Cement
Calcite Cement
Mylonite
Replacement phase
Void-filling cements
Adriatic distal margin
(Incerpi 2017; Incerpi et al., 2017, 2018, 2019)
Galicia distal margin
(Boillot et al., 1988)

Fig. 9

Table 1 O–C, Sr, T_h and U-Pb isotopic data of the analyzed samples belonging to the study area

Sample	$\delta^{13}C$ ‰ VPDB	$\delta^{18}O$ ‰ VPDB
BD—host dolomite		
MAR 23	3.29	−6.77
MAR 8	2.62	−4.52
MAR 33	2.27	−3.84
MAR 39	2.61	−7.79
MAR 30	2.67	−10.78
RI 9	3.05	−6.51
MB 2	2.95	−3.37
BD—dolomite cement		
MAR 8	1.61	−9.25
MAR 39	1.38	−8.60
MAR 33	2.16	−9.32
MB 2	1.81	−12.10
Mylonites—marbles		
MAR 37	2.06	−6.87
MAR 38	1.67	−1.11
MAR 5	3.09	−6.71
MAR 3	1.11	−7.86
BL—host limestone		
RI 1	1.19	−1.26
RI 1	1.17	−1.79
RI 5	0.82	−1.09
MAR 43	2.58	−7.37
MAR 2	2.39	−5.29
MAR 10	2.57	−7.37
BL—calcite cement		
MAR 10	0.97	−7.66
RI 11	1.61	−6.54
MB 2	−1.97	−13.62

Sample	Sr	2σ
BD host dolom	0.73204	0.00051
BD dol cement	0.72145	0.00029
BD host dolom	0.70985	0.00018
BD dol cement	0.70972	0.00024
BL host limest	0.71395	0.00018
BL calcite cem	0.7173	0.00012
BL marble	0.72155	0.00024
BL mylonite	0.71456	0.00013
BL mylonite	0.71516	0.00026
BL mylonite	0.71149	0.01139
BL mylonite	0.71392	0.00021

Sample	U–Pb	2σ
BD host dolom	143.5	9.1
BD dol cement	102	40
BL host limest	122	16
BL calcite cem	95.7	3.4
BL mylonite	90.3	4.9

Table 1

Table 1 (continued)

Sample	U–Pb	2σ
BL mylonite	93.9	3.5
Sample	T_h (°C)	
BL—calcite cement		
Mar 10–26	139.8	232.8
	196.2	240.7
	203.7	240.2
	216.2	243.3
	218.3	244
	219.8	244.7
	223.8	245
	224.7	245.2
	225	249.2
	225	249.3
	227.9	253.7
	228.9	257.2
BL—dolomite cement		
Mar 25	136.6	162.7
	137.7	177.3
	152.2	173
	138.9	185.8
	155	180.2
	163.3	175.7
	181.3	190.2
	184.6	191.4
	187.4	179.4
	203.1	186
	163.3	189.9
	164	195.9
	166.1	194.8
	172.8	181.2
	172.9	185.3
	171.2	181.8
	179.9	182
	184.7	
Marble		
Mar 05	112.8	239.8
	128.9	240.1
	142.1	241.3
	142.2	242.6
	149.8	242.7
	159.8	243.9
	160.8	244.2
	166	245
	169.6	245.1
	169.8	245.3
	175.8	245.3
	187.7	245.4
	191.2	249.8
	192.8	250.2

Table 1 (continued)

Sample	T_h (°C)	
	218	255.3
	220	255.4
	239.6	262.6
Mylonite		
Mas07	114.4	196.2
	116	206.2
	125.7	209.8
	126.8	210
	139.8	217
	165.7	217.1
	169.2	220.6
	169.8	240.2
	171	240.3
	174.8	242.8
	176.2	243
	178.8	243.2
	178.9	244.7
	180.5	253.2
	190.1	255
	190.4	261
	191.3	264.8
	194.8	300.8
	196	
BD—dolomite cement		
Mas34	171.9	229
	180	229.2
	188.8	229.8
	194.8	230.2
	204.7	230.7
	204.8	230.9
	210.2	231
	211.1	231.2
	212.5	232.6
	213.2	232.6
	216	234.7
	220.8	234.8
	222	236.8
	222.8	239.7
	223.6	239.8
	225	245.6
	227.8	247.2
	228.8	248

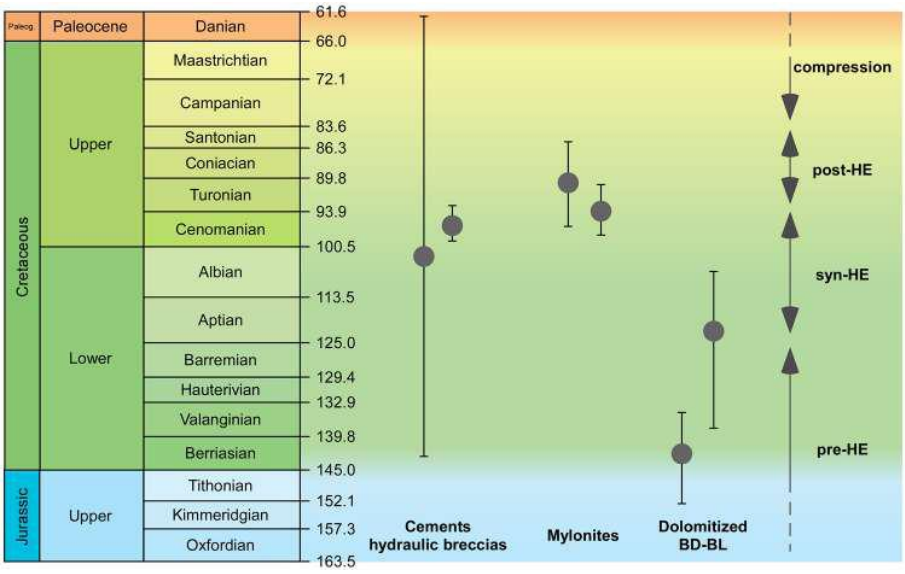
Paleog.
Paleocene
Danian
Cretaceous
Upper
Maastrichtian
Campanian
Santonian
Coniacian
Turonian
Cenomanian
Lower
Albian
Aptian
Barremian
Hauterivian
Valanginian
Berriasian
Jurassic
Upper
Tithonian
Kimmeridgian
Oxfordian
61.6
66.0
72.1
83.6
86.3
89.8
93.9
100.5
113.5
125.0
129.4
132.9
139.8
145.0
152.1
157.3
163.5
compression
post-HE
syn-HE
pre-HE
Cements
hydraulic breccias
Mylonites
Dolomitized
BD-BL

Fig. 11

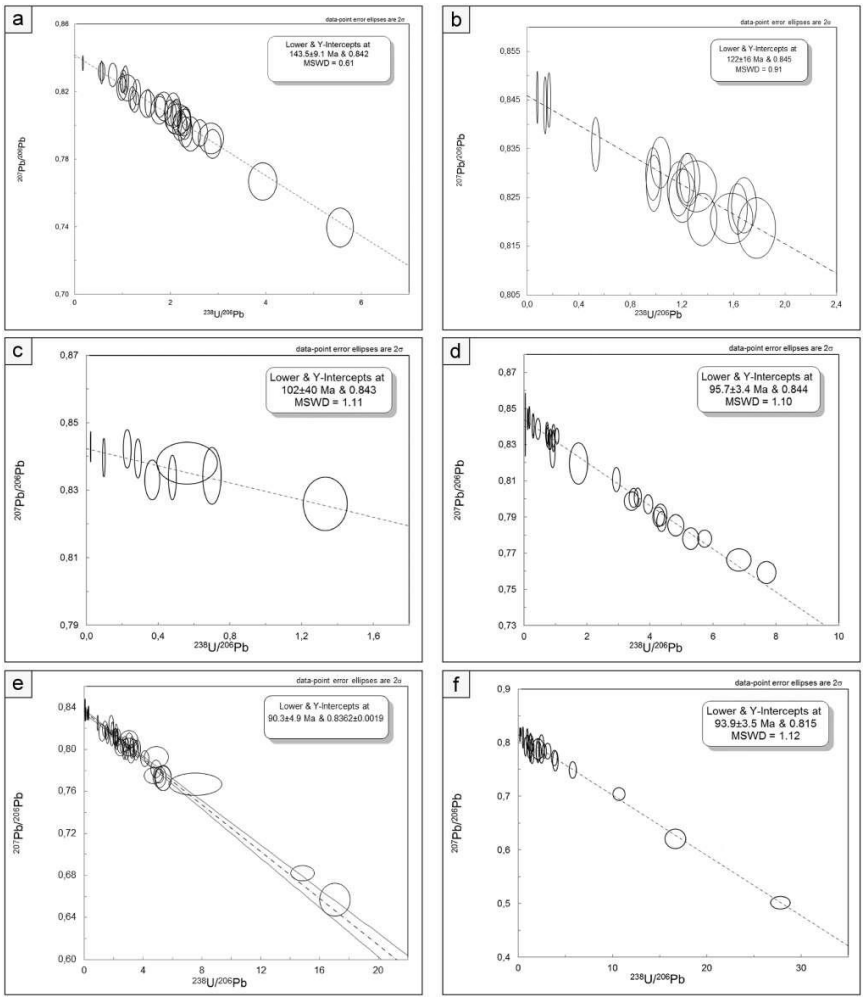
a
Lower & Y-Intercepts at
143.5±9.1 Ma & 0.842
MSWD = 0.61
b
Lower & Y-Intercepts at
122±16 Ma & 0.845
MSWD = 0.91
c
Lower & Y-Intercepts at
102±40 Ma & 0.843
MSWD = 1.11
d
Lower & Y-Intercepts at
95.7±3.4 Ma & 0.844
MSWD = 1.10
e
Lower & Y-Intercepts at
90.3±4.9 Ma & 0.8362±0.0019
f
Lower & Y-Intercepts at
93.9±3.5 Ma & 0.815
MSWD = 1.12
data-point error ellipses are 2σ
207Pb/206Pb
238U/206Pb

Fig. 12

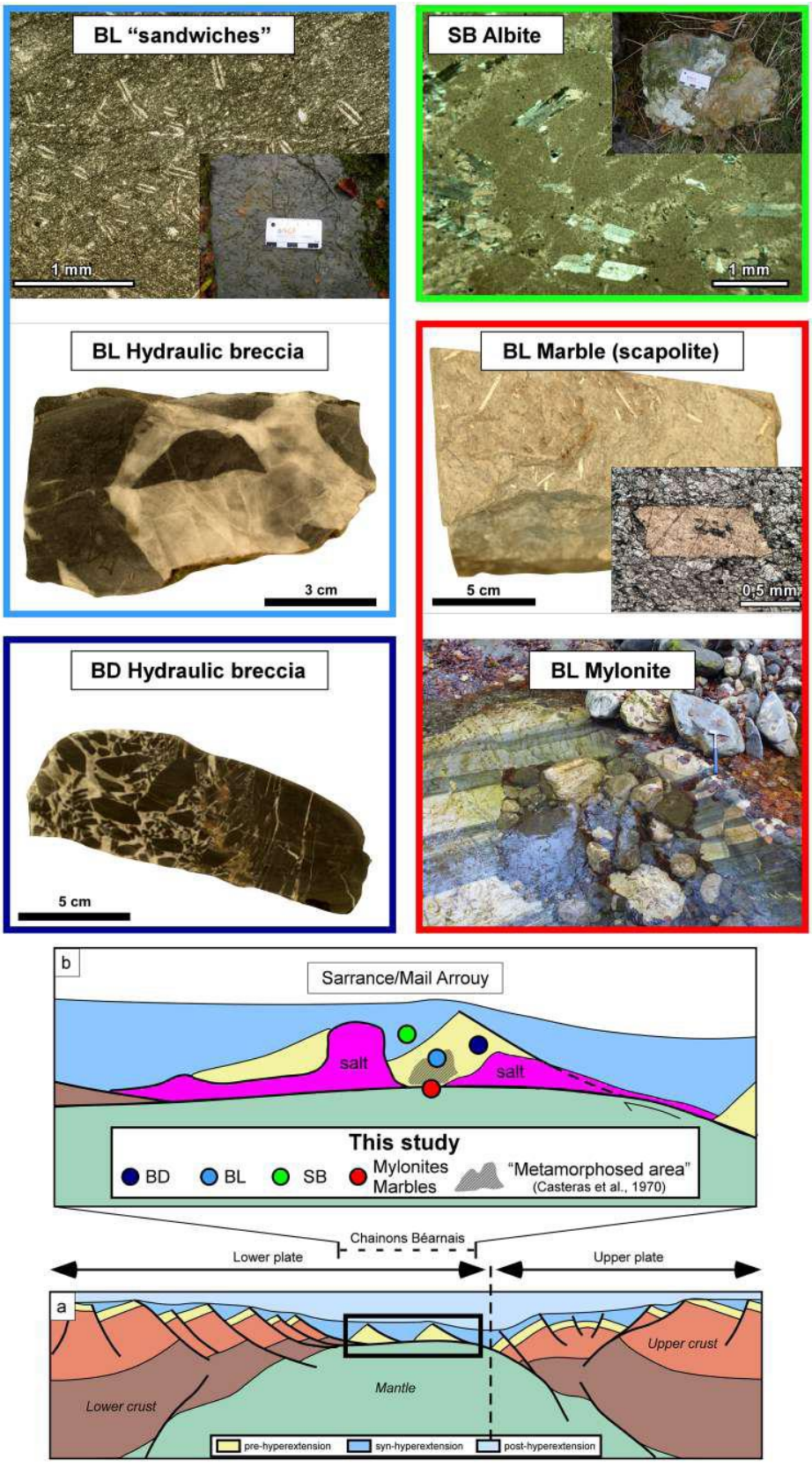
BL "sandwiches"
1 mm
SB Albite
1 mm
BL Hydraulic breccia
3 cm
BL Marble (scapolite)
5 cm
0.5 mm
BD Hydraulic breccia
5 cm
BL Mylonite
b
Sarrance/Mail Arrouy
salt
salt
This study
BD
BL
SB
Mylonites
Marbles
"Metamorphosed area"
(Casteras et al., 1970)
Chainons Béarnais
Lower plate
Upper plate
a
Upper crust
Mantle
Lower crust
pre-hyperextension
syn-hyperextension
post-hyperextension

Fig. 13